Immunity

T follicular helper cells have distinct modes of migration and molecular signatures in naïve and memory immune responses

--Manuscript Draft--

Manuscript Number:	IMMUNITY-D-14-00778R2
Full Title:	T follicular helper cells have distinct modes of migration and molecular signatures in naïve and memory immune responses
Article Type:	Research Article
Keywords:	T follicular helper cell; germinal center; follicular memory T cell; subcapsular sinus macrophages; CD169; EBI2
Corresponding Author:	Tri Phan Garvan Institute of Medical Research Sydney, NSW AUSTRALIA
First Author:	Dan Suan
Order of Authors:	Dan Suan
	Akira Nguyen
	Imogen Moran
	Katherine Bourne
	Jana R Hermes
	Mehreen Arshi
	Henry R Hampton
	Michio Tomura
	Yoshihiro Miwa
	Anthony D Kelleher
	Warren Kaplan
	Elissa D Deenick
	Stuart G Tangye
	Robert Brink
	Tatyana Chtanova
	Tri Phan
Abstract:	B helper follicular T (Tfh) cells are critical for long-term humoral immunity. However, it remains unclear how these cells are recruited and contribute to secondary immune responses. Here we show that primary Tfh cells segregate into follicular mantle (FM) and germinal centre (GC) subpopulations that display distinct gene expression signatures. Restriction of the primary Tfh subpopulation in the GC was shown to require EBI2 downregulation. Following collapse of the GC, memory T cells persisted in a unique niche in the outer follicle where recall responses were initiated by CD169+ subcapsular sinus macrophages. In contrast to the primary response, secondary Tfh cells were not spatially restricted but expanded intrafollicularly before undergoing extrafollicular dissemination via the lymphatic flow. These data suggest that Tfh cells integrate their antigen experience history to focus T cell help within the GC during primary responses, but act rapidly to provide systemic T cell help after re-exposure to the antigen.
Suggested Reviewers:	Pam Schwartzberg pams@nhgri.nih.gov Expertise in Tfh cell biology

	Shane Crotty shane@liai.org Expertise in Tfh biology and immunological memory
	Rafi Ahmed rahmed@emory.edu Expertise in Tfh cells, vaccines and immunological memory
Opposed Reviewers:	Michel Nussenzweig Rockefeller University Direct competitor
	Gabriel Victora Whitehead Institute for Biomedical Research Direct competitor
	Michael McHeyzer-Williams Scripps Research Institute Direct competitor

384 Victoria Street
Darlinghurst NSW 2010
Australia

t: 61 2 9295 8100
f: 61 2 9295 8101

GARVAN INSTITUTE
Breakthrough Medical Research

2nd February 2014

Dr Elizabeth Thompson
Associate Editor
Immunity

Dear Liz,

Thank you for the opportunity to revise our manuscript again for Immunity. We have added new data and analyses and made the required changes to the manuscript after carefully taking into account the Reviewers' comments and your editorial advice.

We hope that everything is now in order and that the manuscript is suitable for publication in *Immunity.*

Thank you for your consideration.

Yours sincerely,

Tri Giang Phan
MBBS, FRACP, FRCPA, PhD
Intravital Microscopy Lab
Immunology Division
Garvan Institute

We thank the reviewers for the additional time and effort needed to critique our revised manuscript. In response, new data and analyses are detailed in the point-by-point response below which also describes the changes to the manuscript. We have also de-emphasised the role of SCS macrophages as advised. Please note that we have broken the response to Reviewer 2 into two sections to cover the initial and subsequent responses.

Reviewer 1

My problem is that this definition does not seem to be applied in a strict manner in the manuscript. For example, p9, "Interestingly, even in this short time period, there was increased accumulation of follicular memory T cells in the subcapsular region in response to the cognate antigen OVA-PE(98% of cells) but not HEL-PE (74% of cells, similar to the 'resting' follicular memory T cells see Fig. 4D) (Figure 5C)". There is no clear evidence showing that these cells are from "follicular memory" cells, but not other 80% memory OT2 cells.

Response: We appreciate this minor concern and the suggestion that the term may cause unnecessary confusion. However, we believe the description of a new population of memory cells warrant a name that captured their unique localization. Nevertheless, we cannot exclude the fact that extrafollicular memory T cells had also relocalized to the subcapsular region as indicated by Reviewer 1. Therefore, we have reworded the reference on p9 to refer to “lymph node resident memory T cells” but kept the term “follicular memory T cells” in other instances where we refer to memory T cells in the follicle prior to their reactivation. Following reactivation we then refer to them as “secondary Tfh cells”.

Change to manuscript:

p.9 main text

- Reworded “Interestingly, even in this short time period, there was increased accumulation of lymph node resident memory T cells in the subcapsular region in response to the cognate antigen OVA-PE (98% of cells in the follicle) but not HEL-PE (74% of cells, similar to the ‘resting’ follicular memory T cells see **Fig. 4D**) (**Figure 5C**).”

Reviewer 2 initial response to revised manuscript

Ise et al. showed multiple findings in disagreement with Suan et al manuscript, none of which are addressed.

Response: In our rebuttal we had tried to avoid detailed discussion of this paper as it uses different methodologies to ours and examines responses in the spleen of “memory Tfh cells” that were FACS-sorted and then adoptively transferred into naïve mice. This is inherently different from our approach which studied the response of persistent antigen-specific cells in the lymph node in immune mice. Nevertheless, we deliberately used this approach as it most accurately models recall (memory) responses in intact immune animals. Thus we do not believe that the contrast of our results with those of Ise *et al*. is somehow problematical as suggested by Reviewer 2. We have revised the manuscript to highlight these differences.
In relation to “memory Tfh cells”, please note that we made great efforts to avoid using this term in our study. Specifically, we examined the recall response of “follicular memory T

cells" in their native environment in immune animals without any ex vivo manipulation. This is important because removal of cells from their niche and the signals that retain them there (such as chemokines, adhesion molecules and survival factors) may cause their subsequent mislocalization upon re-transfer. This, together with the trapping of a proportion of the 1-2 x 10^4 transferred "memory Tfh cells" in other sites such as the lungs, may explain the small numbers of cells recovered and the weak and variable memory responses that were observed by Ise *et al.* (eg. the response they generated from congenically marked memory Tfh cells varied from as little as 8% in Fig. 5B to maximum of 29% in Fig. 4A). In contrast, we obtained consistent, robust responses from as few as 20-100 follicular memory T cells residing in the lymph node, peaking at ~60%, and these cells expressed uniformly very high levels of CXCR5 and PD-1 (revised Suan et al. Fig. S5).
In addition to these methodological differences, we are concerned that the conclusions of Ise et al. may be overstated by Reviewer 2. For example, using adoptive transfers, Luthje et al. (*NI* 2012; 13:491-498) and Weber et al. (*EJI* 2012; 42:1981-1988) were also able to generate much stronger memory responses than Ise *et al*. but in the absence of any memory B cells. Thus, whilst we agree with Reviewer 2 that the data from Ise *et al.* suggest memory B cells may support responses from "memory Tfh cells", the literature clearly shows that they are not necessary for a vigorous secondary Tfh response.

Changes to manuscript:

p.15

- Deleted "However, Ise *et al*. did not exclude a role for splenic $CD169^+$ metallophilic macrophages in that study and it will be interesting to determine if memory B cells also localise to the subcapsular region in the lymph node and are able to activate follicular memory T cells in the absence of SCS macrophages."
- Replaced with "However, these experiments examined recall responses in the spleen of naïve recipient mice following adoptive transfer of FACS-sorted "memory T_{fh} cells". In contrast, we examined the *in situ* recall responses made by persistent antigen-specific cells in the lymph node of immune animals without any *ex vivo* manipulation. It should also be noted that other groups have been able to generate robust memory responses in naïve recipient mice without the need for co-transfer of memory B cells (Luthje et al., 2012; Weber et al., 2012). Hence, while memory B cells may support secondary T_{fh} responses at the T-B border under some circumstances, it is likely that local responses in draining lymph nodes can also generated be in the subcapsular region."

Ise et al. : Resting memory Tfh cells—directly defined by adoptive transfer--are located throughout the follicle, and predominantly at the T-B border.
Suan et al: "Memory Tfh cells" by their definition selectively localize almost exclusively next to the subcapsular sinus.

Response: We were very careful to avoid using the term "memory Tfh cells" as technical reasons prevented us from phenotyping and tracking the ontogeny of these cells. However, we did state a clear definition in our revised manuscript: "Nevertheless, we have used the term "follicular memory T cell" purely to denote their location inside the follicle (in contrast to the extrafollicular memory T cells) without making any assumptions about their origin or relationship to Tfh cells." Thus, our definition is inclusive of the cells described by Ise *et al.* in the follicle and T-B border.

Ise et al. : Memory Tfh cells are reactivated at the T-B border
Suan et al: Memory Tfh cells are reactivated at the subcapsular sinus.

Response: Please see comment 1 above regarding differences between the response detailed by Ise *et al.* in the spleen and the responses that we tracked in the lymph node. Importantly, as we have tried to point out, the conclusions of Ise *et al.* and Suan *et al.* are not mutually exclusive.

Ise et al: Memory Tfh cells are reactivated by memory B cells
Suan et al: Memory Tfh cells are reactivated by SCS macrophages.
Ise et al. shows direct experimental evidence of antigen presentation by memory B cells, and up regulation of Bcl6 by the activated memory Tfh cells. Suan et al do not.

Response: With all due respect, we feel the data Reviewer 2 refers to from Ise *et al.* is rather indirect. In particular, Ise *et al.* Fig. 5A and 5B only show that detectable peptide:MHCII increases from a baseline level of 8.9% in naïve B cells to 17% in memory B cells. Thus, the data could also indicate activation of the transferred memory Tfh cells by naïve B cells. Notably, at no point do they show any co-localisation of memory B cells and memory Tfh cells (eg they only show a few Bcl6+ T cells at the T-B border in Fig. 2D but do not show them in contact with memory B cells). In addition, they do not show any evidence for direct interactions with memory B cells. In contrast, we have directly visualised secondary Tfh cell activation by SCS macrophages by intravital two-photon microscopy. Furthermore, we also have single cell RT-qPCR data showing that both optically marked and sorted populations of secondary Tfh cells express high levels of Bcl6; this data can be added if the editor deems it appropriate and necessary.

My response: I disagree. (1) This is a slight change in 5c. Also, their definition of "KD OT2 in proximity to SCS" is confusing here, because in Fig 4B the majority of KD OT2 cells are outside of the follicle or SCS, so in 5c are the authors only referring to a subset of the total cells, and if so how are they making the distinction for which cells to count?

Response: We believe the result in Suan *et al.* Fig. 5C not a “slight change” but is in fact a near maximal response. We show that 75% of the follicular memory T cells localize in the subcapsular region with non-cognate antigen and this increases to nearly 100% with cognate antigen (p=0.0077). Since it is not possible to achieve >100% retention, we believe that this difference is quite marked and almost the maximum that can be achieved. In these analyses the denominator is the number of KD OT2 memory cells in the whole follicle.

At any rate, this observation is in contradiction to the published work of Ise et al., discussed above, where the memory Tfh cells predominantly receive signals at the T-B border (Ise et al, Figure 2D).

Response: Again, we cannot find any evidence in Ise *et al.* that show “memory Tfh cells predominantly receive signals at the T-B border”. Ise *et al.* Fig. 2D only shows a few Bcl6+ T cells at the T-B border – they do not provide any evidence to show that these cells are antigen activated, that memory B cells co-localize there, or that this is indeed the site of their activation. It is possible, for example, that the cells are reactivated in another location and then rapidly relocalize to the T-B border by the time the images are taken. In any event, as we have pointed out, the data obtained by Ise *et al.* using a cell transfer system in no way invalidates our findings using an intact recall response.

The claim that a more rounded morphology can be directly interpreted as "TCR activation" is a stretch well beyond the data they have.

Response: Initial in vitro and sunsequent in vivo imaging experiments have clearly established that T cells receive a "TCR stop signal" upon antigen engagement (eg Dustin et al. *PNAS* 1997; 94:3909-3913; Miller et al. *Science* 2002; 296:1869-1873, Mempel et al. *Nature* 2004; 427:154-159; Cahalan & Parker *Annu Rev Immunol* 2008; 26:585-626) and this is associated with acquisition of a rounded cell morphology (eg Donnadieu et al. *Current Biology* 1994; 4:584-595; Negulescu et al. *Immunity* 1996; 4:421-430; Okada et al. *PLOS Biology* 2005: 3(6):e150; Mrass et al. *Immunity* 2008; 29: 971-985). Therefore, our direct visualization by two-photon microscopy that the cells in the subcapsular region have stopped moving (Movie S5) and are more likely to be arrested (Suan et al. Fig. 5F) and have a rounded morphology (Fig. 5E) is consistent with a substantial body of literature indicating that this results from TCR activation and formation of the immunological synapse. We now provide additional image analysis showing a cell receiving a TCR stop signal upon contact with an SCS macrophage and forming a stable long term conjugate.

Changes to manuscript:

- New figure panel **Figure 5D** shows example of a cell slowing down and stopping in contact and forming stable conjugate with SCS macrophages.

p.9 main text

- Reworded "Time-lapse two-photon microscopy of draining lymph nodes 2 days after rechallenge with OVA showed secondary T_{fh} cells slowed down and stopped migrating when they came into contact with SCS macrophages (**Figure 5D**), in contrast to the active scanning by 'resting' follicular memory T cells before antigen recall (**Figure 4H**). Accordingly, secondary T_{fh} cells in the subcapsular region had a rounded morphology and higher arrest coefficient than those in the inner follicle (**Figures 5E, F and G,** and **Movie S5**) suggestive of TCR engagement."

The authors do not show "cells actually undergoing cell division," as they repeatedly state. They showed a single cell dividing. One single event. That cell is also in the follicle, defined by the CD157 FDC staining, which overlaps that cell.

Response: In addition to Fig 5G and Supplemental Movie S5, we also show KD OT2 cell dividing in contact with the process of an SCS macrophage in Supplemental Movie S6. We did not add more movies showing cells dividing on SCS macrophages as it was considered superfluous but have added another example of cell dividing in Supplemental Movie S5. The CD157 appears to overlap because it is a maximal intensity projection over multiple z-stacks.

Changes to manuscript:

- Edited **Supplemental Movie S5** to add another example of cell dividing

In the original critique I wrote: "Nor do they have an explanation for why and how the cells exit into the lymph and then reenter from the lymph."…
My response: That reply is all simply speculation. The authors do not know mechanism.

Response: We are actively pursuing the molecular mechanisms for this novel migration pattern. However, the molecular profiling data does suggest a potential insight which we have added to the data. Specifically, the single cell transcript data shows the regulator of

G protein signaling molecule RGS16 is markedly induced in primary GC Tfh cells but not in secondary Tfh cells. RGS16 has been shown to be induced by FDCs (Estes JI 2004; 173:6169-78) and mediate GC positioning of Tfh cells (Ding JI 2013; 191:1614-24). Therefore, it is possible that RGS16 may act to reduce chemokine responsiveness of primary GC Tfh cells and thereby retain them in the FDC-rich light zone of the GC, whereas secondary Tfh cells are able to respond to any number of chemokines and migrate out of the GC and subsequently out of the follicle. We suspect that this additional layer of control allows the cells to integrate the multiple changes in chemokine responsiveness to determine their global positioning and are actively pursuing it. I should add we have been reluctant to present this data because it would take a considerable amount of time to follow up with more definitive functional experiments. This would involve importing the necessary RGS16 transgenic and knockout mice and crossing them with our KD OT2 and chemokine receptor knockouts (such as EBI2 knockout). Therefore, we feel that such a long term stand-alone project (taking >12 months) would be well outside the scope of the current manuscript.

Changes to manuscipt:

- New data panel **Figure 7D** showing expression of *Rgs16* is specifically induced in primary but not secondary Tfh cells.

p.10 main text

- Added "Furthermore, selective induction of the regulator of G-protein signaling family member *Rgs16* (Estes et al., 2004) in primary GC T_{fh} cells was also absent in the secondary response (**Figure 7D**)."

p.14 main text (discussion)

- Added "Furthermore, *Rgs16* was induced in primary but not secondary GC T_{fh} cells, suggesting an additional layer of control in chemokine receptor signaling allows the cells to integrate the changes in expression of these and possibly other chemokine receptors to determine their global positioning."

My response: That is not a compelling argument. The only difference shown was an EBI2 mRNA difference of 3 versus 4 arbitrary units. That is less than a two-fold difference, and seems unlikely to be responsible for the dramatic intermolecular migration observed. Furthermore, the authors show no EBI2 protein data to directly demonstrate EBI2 expression on the cells in the secondary immune response.

Response: We apologize if it was not made clear that the expression level is in log2. The actual value is 4.85 for GC Tfh and 2.93 for FM Tfh ie a nearly 4-fold difference (p<0.0001). However, the comment that this difference "*seems unlikely to be responsible for the dramatic intermolecular migration observed"* stands in marked contrast to the data we presented Fig. 3 of the original and revised manuscripts detailing functional studies with EBI2 KO and EBI2 overexpressing OT2 T cells. We did not detect a difference in *Gpr183* expression in the secondary response and therefore did not pursue protein expression (although we did carefully document dynamic changes in EBI2 protein expression in the primary response in Fig. 3). Nevertheless, despite the absence of any difference in *Gpr183* expression levels in secondary Tfh cells, we did compare the secondary Tfh response of EBI2 KO and wildtype KD OT2 T cells as requested by Reviewer 2 but found no differences.

Change to manuscript:

- Added $\log_2$ to axis label in **Figure 7B, C and D** to indicate this more clearly.

The single cell qPCR data in Figure 7B have very tight error bars. I have only seen tight error bars for single cell PCR when genes are very highly expressed, e.g. housekeeping genes. For most genes, there are a high frequency of negative cells. One example paper is Arsenio, J., et al (2014). Early specification of CD8(+) T lymphocyte fates during adaptive immunity revealed by single-cell gene-expression analyses. Nature Immunology, 15(4), 365-372. doi:10.1038/ni.2842. Is the reader to conclude from this that CCR7 and Gpr183 (Ebi2) are highly expressed in all CD4 T cells?

Response: We are excited by the robustness and reproducibility of our multiplex single cell RT-qPCR assay (see Supplemental Figure S5 in original submission which unfortunately had to be removed because of space in revised manuscript). The extremely tight error bars is a testament to this and also the fact that we had such a large number of replicates. We can confirm that *Ccr7* and *Gpr183* is expressed by the majority of the cells and that only a few cells that did not amplify the gene. We have changed the figure to show individual data points.

Change to manuscript:

- **Figure 7B, C and D** have been changed to scatter plot to show expression levels for individual cells.

My reply: In contrast to what the authors state, no data on confinement are actually shown in Figure S1.

Response: Reviewer 2 was concerned that SAP KO recipients skewed the observed response and was not convinced by the kinetics of the response in wild-type mice as shown in revised Fig. S1 and asks for the confinement data. We have now added a new panel **Supplemental Figure S1E** showing confinement of primary Tfh cells in wildtype recipients.

Change to manuscript:

- New panel **Supplemental Figure S1E** showing response of KD OT2 T cells in wildtype recipient mice. Tracks of FM and GC Tfh cells demonstrate tight spatial segregation of the two subpopulations.

Reviewer 2 second response to revised manuscript

Regarding the value of adoptive transfers, range of 8%-29% is actually a reasonably tight range for T cell response. I don't see that any one of these model is more physiological than the other. Yuan and Ise both use OTII TCR transgenic cell transfer system.

Response: While we both use OT2 TCR transgenic cells, as we discussed above Ise et al. go on to isolate and adoptively transfer their "memory Tfh cells" into naïve mice before rechallenge. In contrast, we leave the cells in situ and rechallenge the mice.

*** This seems to be talking in circles. However they define the cells, they do not**

appear to see them at the T-B border at any significant frequency—instead they were in the subcapsular sinus. In contrast, Ise et al. observed the majority of the memory cells at the T-B border.

Response: This is the point of our result – in the draining lymph nodes of immune mice, memory T cells are reactivated in the subcapsular region and not the T-B border.

Not at all! The restimulation of the memory Tfh cells did not occur without the transfer of memory B cells, and furthermore did not occur without the transfer of antigen-specific memory B cells.

Response: The point we were trying to make was that the "direct experimental evidence for antigen presentation by memory B cells" was at best indirect and weak. We do not dispute that Ise et al. could not generate a secondary response without antigen-specific memory B cells. However, we would like to again point out that Luthje et al. and Weber et al. were able to generate much better responses using similar adoptive transfer systems into naïve mice without memory B cells.

This is a fair point. Though, of course, the cells are in contact with B cells at the T-B border. But the key overall point I was making is that in Ise et al. they show a mechanism. The reactivation was dependent on antigen-specific memory B cells, based on cell transfers. As I have said over and over, Yuan et al. has no data on mechanism. Seeing T cells near SCS macrophages does not suffice.

Response: We have de-emphasised the role played by SCS macrophages in reactivation of follicular memory T cells.

Change to manuscript:

p.8

- Changed title of result from **"Follicular memory T cells are by SCS macrophages upon antigen recall"**
- to **"Follicular memory T cells are activated in the subcapsular region upon antigen recall"**

p.9

- Changed text from "Thus, SCS macrophages are able to capture and present antigen to follicular memory T cells to initiate the secondary immune response."
- to "Thus, the secondary immune response in lymph node is initiated in the subcapsular region."

p.15

- Changed "Thus, the finding that follicular memory T cells are activated to proliferate by SCS macrophages also resolves the question of how and where the secondary antibody response is initiated."
- to "Thus, the finding that follicular memory T cells are activated to proliferate in the subcapsular region also resolves the question of how and where the secondary antibody response is initiated."

p.15

- Added "Hence, while memory B cells may support secondary T_{fh} responses at the T-B border under some circumstances, it is likely that local responses in draining lymph nodes

can also be generated in the subcapsular region."

p.24

- Changed Figure 5 title **"Follicular memory T cells are activated by SCS macrophages."**
- to **"Follicular memory T cells are activated in the subcapsular region."**

*** The cells are already sessile, so I find these arguments insufficient for defining which cell is the APC. A manipulation of the APC is necessary to show that it is the APC, or a demonstration of synapses.**

Response: We originally highlighted 2 cells that had arrested in Supplemental Movie S5 to contrast them with active scanning of SCS macrophages before antigen recall in Supplemental Movie S4. We have now added tracking data to new **Figure 5D** to show that the cells are not sessile but motile until they contact SCS macrophages at which point they slow down and form stable conjugates.

Change to manuscript:

- New **Figure 5D** panel.

p.9 main text

- Reworded text "Time-lapse two-photon microscopy of draining lymph nodes 2 days after rechallenge with OVA showed secondary T_{fh} cells slowed down and stopped migrating when they came into contact with SCS macrophages (**Figure 5D**), in contrast to the active scanning by 'resting' follicular memory T cells before antigen recall (**Figure 4H**). Accordingly, secondary T_{fh} cells in the subcapsular region had a rounded morphology and higher arrest coefficient than those in the inner follicle (**Figures 5E, F and G,** and **Movie S5**) suggestive of TCR engagement."

*** Fig 5G and Movie s5 are the same cell. Movie S6 is a second cell I presume. The point is, what percentage of division events are associated with SCS versus other cells?**

Response: We did not observe cell division at the T-B border or inner B cell follicle. We have edited **Supplemental Movie S5** to add another example of a cell dividing.

Change to manuscript:

- Edited **Supplemental Movie S5** to add another example.

*** Showing individual data points would increase confidence in these novel results.**

Response: We have amended the figure to show individual data points.

Change to manuscript:

- Ameneded **Figure 7B, C and D** to show individual data points.

T follicular helper cells have distinct modes of migration and molecular signatures in naïve and memory immune responses

Running title: **T_{fh} cell dynamics in naïve and immune animals**

Dan Suan[1,2*], Akira Nguyen[1,2*], Imogen Moran[1,2*], Katherine Bourne[1], Jana R. Hermes[1], Mehreen Arshi[1,3], Henry R. Hampton[1,2], Michio Tomura[4], Yoshihiro Miwa[5], Anthony D. Kelleher[3], Warren Kaplan[1,2], Elissa K. Deenick[1, 2], Stuart G. Tangye[1,2], Robert Brink[1,2], Tatyana Chtanova[1, 2] and Tri Giang Phan[1, 2]

Affiliations: [1] Garvan Institute of Medical Research, Sydney, Australia; [2] St Vincent's Clinical School, Faculty of Medicine, UNSW Australia, Sydney, Australia; [3] St Vincent's Centre for Applied Medical Research, Sydney Australia; [4] Kyoto University Graduate School of Medicine, Kyoto, Japan; and [5] University of Tsukuba, Tsukuba, Japan.

*These 3 authors contributed equally to this work

Correspondence to: Dr Tatyana Chtanova, email: t.chtanova@garvan.org.au, or

Dr Tri Giang Phan, email: t.phan@garvan.org.au

SUMMARY

B helper follicular T (T_{fh}) cells are critical for long-term humoral immunity. However, it remains unclear how these cells are recruited and contribute to secondary immune responses. Here we show that primary T_{fh} cells segregate into follicular mantle (FM) and germinal centre (GC) subpopulations that display distinct gene expression signatures. Restriction of the primary T_{fh} subpopulation in the GC was shown to require EBI2 downregulation. Following collapse of the GC, memory T cells persisted in a unique niche in the outer follicle where recall responses were initiated by $CD169^+$ subcapsular sinus macrophages. In contrast to the primary response, secondary T_{fh} cells were not spatially restricted but expanded intrafollicularly before undergoing extrafollicular dissemination via the lymphatic flow. These data suggest that T_{fh} cells integrate their antigen experience history to focus T cell help within the GC during primary responses, but act rapidly to provide systemic T cell help after re-exposure to the antigen.

INTRODUCTION

The production of neutralizing antibodies by long-lived plasma cells and memory B cells upon antigen re-exposure underpins the protection afforded by most successful vaccines (Plotkin, 2008). These outputs from the germinal centre (GC) are critically dependent on sequential $CD4^+$ T cell help provided to B cells at multiple sites including the interfollicular zone (Kerfoot et al., 2011), T-B border (Garside et al., 1998; Okada et al., 2005) and within GCs (Allen et al., 2007; MacLennan, 1994; Victora and Nussenzweig, 2012) to drive antibody affinity maturation and memory formation (Crotty, 2011). The term follicular B helper T cells (T_{fh}) was originally used to describe human $CD4^+$ T cells that express the chemokine receptor CXCR5, localize to the secondary follicle of tonsils and provide cognate help to B cells (Breitfeld et al., 2000; Schaerli et al., 2000). The importance of T_{fh} cells to human health is underscored by the recurrent bacterial infections that occur when they are defective, and the autoimmune pathologies that develop when they are in excess (Tangye et al., 2013). Rapid developments in the T_{fh} field in recent years has been facilitated by the use of cell surface molecules, such as CXCR5, PD-1 and ICOS (Haynes et al., 2007; Rasheed et al., 2006), as surrogate markers for tracking T_{fh} cells in human subjects and genetic mouse models. Unfortunately, these markers of $CD4^+$ T cell activation are not unique to T_{fh} cells. For example, CXCR5 is upregulated by multiple $CD4^+$ T cell lineages upon activation *in vivo* (Ansel et al., 1999; Schaerli et al., 2001). Nevertheless, the recognition that the transcriptional repressor Bcl-6 is absolutely required for T_{fh} cell development firmly established them as a distinct $CD4^+$ T cell lineage (Chtanova et al., 2004; Johnston et al., 2009; Nurieva et al., 2009; Yu et al., 2009). However, Bcl-6 expression is also not T_{fh} cell-specific as it is upregulated in all dividing $CD4^+$ T cells during their interactions with dendritic cells (DCs) (Baumjohann et al., 2011; Kitano et al., 2011). Taken together, these uncertainties make it difficult to conclusively track the origin and fate of T_{fh} cells in the primary and secondary antibody response.

Recently, a method for *in vivo* photoactivation of cells expressing PA-GFP in precise microanatomical compartments was described (Victora et al., 2010), which makes it possible to

optically mark T_{fh} cells and track them 20 hours later (Shulman et al., 2013). Unexpectedly, they reported that T_{fh} cells frequently migrated out of the follicle to invade neighbouring GCs, and proposed that this promoted affinity maturation by providing a diverse polyclonal source of $CD4^+$ T cell help (Shulman et al., 2013). However, the temporospatial context of such promiscuous behaviour was not defined. We have developed an alternative method for optical marking by two-photon photoconversion (TPP) of cells expressing the photoconvertible fluorescent protein Kaede (KD) (Chtanova et al., 2014). Our studies using TPP show striking differences in the migration and behaviour of T_{fh} cells during three distinct phases: the primary response by naïve $CD4^+$ T cells; the memory phase following resolution of the GC response; and the secondary response by antigen-experienced cells. We demonstrate the migration of GC T_{fh} cells in the primary response was confined to the GC of origin and infrequently observed to cross into the follicular mantle (FM), a distinct region in the follicle surrounding the GC (Hardie et al., 1993). Follicular memory T cells were tracked to the outer follicle where they scanned $CD169^+$ macrophages lining the subcapsular sinus (SCS) and become activated to divide upon antigen rechallenge. Remarkably, there was unrestricted movement of GC T_{fh} cells in the secondary response, and we show that they also enter and leave the follicle via the lymphatic flow in the SCS. Finally, we use TPP and single cell gene expression and functional analyses to show that the temporospatial cues guiding the positioning of T_{fh} cells during these phases of the immune response were provided by Epstein-Barr virus-induced G-protein coupled receptor 2 (EBI2).

RESULTS

Spatial segregation of primary T_{fh} cells in the FM and GC

To track T_{fh} cells, we adoptively transferred KD OT2 $CD4^+$ T cells into recipient mice deficient for SLAM-associated protein (SAP) (Czar et al., 2001), and immunised them subcutaneously with chicken ovalbumin (OVA). The expansion of $CXCR5^+CCR7^{lo}PD\text{-}1^+$ cells in the draining lymph node was used to track T_{fh} cell kinetics and this peaked on day 5, two days before the peak of GC B cells (**Figure S1**). Similar kinetics were obseved in wildtype recipinet mice (**Figure S1**). This was

confirmed by histology and FACS analysis of optically marked cells, which showed that the follicle is extensively colonised by $CXCR5^{+}CCR7^{lo}PD\text{-}1^{+}$ T_{fh} cells on day 5, before mature GCs have formed (**Figure S2** and data not shown). Previously we labeled follicular stromal cells *in vivo* by injecting anti-CD157 mAb the day before imaging (Phan et al., 2007). We now report that anti-CD157 injected subcutaneously 3-4 days prior to imaging results in contraction of the anti-CD157 signal to colocalize with IgD^{lo} antigen-specific GC B cells, peanut aggluttinin (PNA), CD35 and FDC-bearing immune complexes. This CD157-rich region excludes IgD^{+} naïve B cells and polyclonal B cells, consistent with classical definitions of GCs (see **Fig. S3** and **Supplemental Experimental Procedures** for description and validation of the labeling strategy). Time-lapse microscopy of the lymph node at the peak of the primary GC response on day 7 showed T_{fh} cells were localised in two separate microanatomical compartments within the follicle (**Figures 1A and B,** and **Movie S1**). Thus, some T_{fh} cells were confined to the GC (ie GC T_{fh} cells) and only infrequently observed to emigrate from the GC to the FM (<10%). Other T_{fh} cells were confined to the FM, and these FM T_{fh} cells were similarly observed to cross over into the GC at a low frequency (<20%). Cell tracking showed both GC and FM T_{fh} cells were highly motile with median instantaneous velocities of 8.5 and 7.8μm/min, and median confinement indices of 0.41 and 0.47, respectively (**Figures 1C and D**). This spatial confinement was confirmed by intravital TPP and discontinuous tracking of the same GC 24 hours later, which showed ~65% of photoconverted GC T_{fh} cells were retained in the original GC and ~33% had migrated into the FM of the original follicle (**Figures 1E-G,** and **Movie S2**). Importantly, in contrast to the findings of Shulman et al., >98% of the photoconverted GC T_{fh} cells were retained in the original follicle, and only a few cells could be found outside in immediately adjacent GCs (see yellow triangles in **Figure 1E**).

Primary GC and FM T_{fh} cells have distinct gene expression signatures

Lymph nodes were then harvested on day 7 and multiple areas in either the GC or FM photoconverted *ex vivo* (**Figure 2A and B**). FACS analysis of photoconverted red cells showed both populations expressed high levels of CXCR5 and PD-1 and low levels of CCR7 (**Figure 2C**

and D). However, while GC T_{fh} cells expressed 2-fold higher levels of CXCR5 and PD-1 than FM T_{fh} cells, there was significant overlap in their expression levels making it difficult to exclusively resolve them by FACS (**Figures 2C and D**). These data show primary GC and FM T_{fh} cells are anatomically distinct T_{fh} subpopulations that are best resolved by location-based optical marking rather than CXCR5 and PD-1 expression.

To further characterise these unique primary T_{fh} cell subpopulations, we optically marked them and performed multiplex single cell RT-qPCR on day 7 for expression of a panel of 32 genes in 64 GC and 62 FM T_{fh} cells (**Figure S4** and **Table S1**). Seven of the 32 genes included as negative controls (*Foxp3, Il2ra, Infg, Prdm1, Rorc, Slamf8* and *Tbx1*) were not expressed by any of the T_{fh} cells and therefore excluded from analysis. GC T_{fh} cells expressed >2-fold higher levels of *Bcl6, Pdcd1, Rgs16, Il21* and *Il4* and >2-fold lower levels of *Ccr7, Cd62l, Gpr183, Btla and Slamf6* than FM T_{fh} cells (**Figure 2E**). We next performed unsupervised dimensionality reduction on the 25 gene × 126 cell matrix by non-negative matrix factorisation (NMF) (Brunet et al., 2004) to determine if the gene expression pattern clustered cells based on their microanatomical location. This analysis showed that the data decomposed most robustly and reproducibly into 2 clusters (rank $k = 2$), as reflected by the high cophenetic correlation coefficient of 0.9995 (**Figure S4**). Analysis of expression of the 2 identified metagenes across samples showed striking partitioning of cells based on their location (**Figures 2F and G**). Interestingly, there was little difference between the original ordering (based on location) and re-ordered samples (based on metagene expression), suggesting that primary FM and GC T_{fh} cells are molecularly distinct and can be defined by expression of metagene P1 or P2, respectively. Accordingly, when samples were plotted by metagene expression it is clear that GC T_{fh} cells are clustered together based on their high expression of metagene P2 and low expression of metagene P1, and FM T_{fh} cells based on their high expression of metagene P1 and low expression of metagene P2 (**Figure 2G**). The large Euclidean distance of 4.47 between the centroid of these clusters reflects their distinct molecular identity. Vector analysis showed that the major unique gene contributors to the metagene P2 (characteristic of GC T_{fh} cells) were *Bcl6,*

Pdcd1 and *Il21*, and metagene P1 (characteristic of FM T_{fh} cells) were *Ccr7* and *Cd62l* (**Figure 2H**). Thus, primary GC T_{fh} cells have a distinct gene expression signature from FM T_{fh} cells.

EBI2 guides the spatial segregation of primary T_{fh} cells in the FM and GC

We noted from the single cell RT-qPCR that expression of *Gpr183*, the gene encoding EBI2, was significantly downregulated in primary GC T_{fh} cells (**Figure 2E**) and therefore determined its surface expression by T_{fh} cells as the immune response progressed (**Figures 3A-C**). Interestingly, EBI2 was initially induced in antigen-specific KD OT2 cells, especially the $CXCR5^+PD\text{-}1^+$ cells, compared to endogenous $CD4^+$ T cells 3 days after immunisation with OVA. It was then downmodulated on day 7 to be expressed at the same level on KD OT2 as endogenous $CD4^+$ T cells. On day 14, when most T_{fh} cells were localised in the GC and few remained outside in the FM, EBI2 was further downregulated in the $CXCR5^+PD\text{-}1^+$ subset. Thus, a clear subpopulation of $EBI2^{lo}$ T_{fh} cells could be detected by day 14 of the primary response (**Figure 3C**). We next optically marked FM and GC T_{fh} cells on day 7 and analysed them by FACS (**Figure 3D**). This showed that EBI2 was specifically downregulated by a subset of GC T_{fh} cells that expressed the highest levels of PD-1. To test the role of EBI2 in primary T_{fh} cell localisation, we retrovirally transduced OT2 T cells with either an empty or EBI2 expression vector (**Figures 3E and F**). Transduced cells expressing GFP were FACS sorted, adoptively transferred into wildtype recipients that were immunised with OVA. When draining lymph nodes were imaged on day 7, EBI2 overexpressing cells preferentially localised to the subcapsular and interfollicular region, and there was a nearly 2-fold reduction in the proportion of transduced OT2 T_{fh} cells in the GC. Conversely, EBI2-deficient KD OT2 T cell were 2.5-fold more efficient than wildtype KD OT2 T cells in localising to the GC (**Figures 3G and H**). Thus, EBI2 provides one of the molecular cues needed to guide primary T_{fh} cells as they navigate between the GC and FM.

Follicular memory T cells patrol the outer follicle and scan SCS macrophages for antigen

We next tracked KD OT2 T cells after resolution of the immune response when the majority of GCs have collapsed. At these late timepoints, while the numbers of KD OT2 T cells have massively

contracted, rare cells (20-200 per lymph node) were still detectable by FACS analysis (see panel on day 28, **Figure S5**). While the majority of these cells were $CCR7^+$ consistent with a central memory phenotype, a small subpopulation were $CXCR5^+$. We therefore injected anti-CD157 mAb the day before imaging to label the B cell follicle and scanned lymph nodes from immune animals to determine the location of these persistent cells (**Fig. 4A** and **Movie S3**). These analyses showed that long-lived KD OT2 T cells could still be detected inside follicles following resolution of GCs where they comprised 20% of the memory cell pool. *In vivo* labeling of subcapsular sinus (SCS) macrophages with CD169 showed that the majority of the KD OT2 cells were located peripherally in the follicle and interfollicular regions (**Fig. 4B** and **Movies S3**). This was confirmed by imaging from both the cortical and medullary side to depths of 360μm (data not shown). Time-lapse two-photon microscopy showed these antigen-specific $CD4^+$ T cells persisting inside the follicle spent most of their time (>75%) in close proximity to SCS macrophages where they migrated with significantly reduced instantaneous velocity, increased arrest coefficient and reduced motility coefficient compared to when they were deeper in the follicle, consistent with antigen surveillance (**Figure 4C-G** and **Movie S4**). Notably, these cells were observed to make extensive surface contacts with SCS macrophages as demonstrated by colocalization analysis (**Figure 4H** and **Movie S4**). Unfortunately, the rarity of these cells and degradation of photoconverted Kaede protein after several weeks (Chtanova et al., 2014) presented major technical challenges to their phenotypic characterisation and lineage tracing. Nevertheless, we have used the term "follicular memory T cell" purely to denote their location inside the follicle (in contrast to the extrafollicular memory T cells) without making any assumptions about their origin or relationship to T_{fh} cells.

Follicular memory T cells are activated in the subcapsular region upon antigen recall

Given the localisation of these memory T cells in the outer follicle we next asked if this was also the site of secondary T_{fh} cell activation. Initially, we used OVA-PE to show that antigen, possibly bound in immune complexes by neutralizing anti-OVA antibodies generated from the initial immunisation, is rapidly transported to the lymph node upon rechallenge where it is captured and

displayed by $CD169^+$ macrophages lining the SCS and interfollicular zones within 4 hours (**Figure 5A and B**). By comparison, there was significantly less capture of the irrelevant antigen hen egg lysozyme (HEL)-PE (to which there were no immune antibodies) in the subcapsular region (**Figure 5A and B**). Interestingly, even in this short time period, there was increased accumulation of lymph node resident memory T cells in the subcapsular region in response to the cognate antigen OVA-PE (98% of cells in the follicle) but not HEL-PE (74% of cells, similar to the 'resting' follicular memory T cells see **Fig. 4D**) (**Figure 5C**). Time-lapse two-photon microscopy of draining lymph nodes 2 days after rechallenge with OVA showed secondary T_{fh} cells slowed down and stopped migrating when they came into contact with SCS macrophages (**Figure 5D**), in contrast to the active scanning by 'resting' follicular memory T cells before antigen recall (**Figure 4H**). Accordingly, secondary T_{fh} cells in the subcapsular region had a rounded morphology and higher arrest coefficient than those in the inner follicle (**Figures 5E, F and G,** and **Movie S5**) suggestive of TCR engagement. We also observed memory T cells undergoing cell division while in contact with SCS macrophages (**Figure 5H** and **Movie S5**). Thus, the secondary immune response in lymph node is initiated in the subcapsular region.

Unrestricted migration of secondary T_{fh} cells out of the GC and lymph node

We next determined the migration pattern and behaviour of secondary T_{fh} cells (**Figure 6A-D)**. Upon antigen recall, a more rapid GC response is generated that peaks on day 5, two days earlier than in the primary response (**Figure S5**). Interestingly, the T_{fh} cell response to secondary antigen is stereotyped by rapid generation of an almost uniform population of $CXCR5^+CCR7^{lo}PD\text{-}1^{hi}$ cells. Remarkably, secondary T_{fh} cells were seen to migrate from the GC to the FM at a 5-fold higher frequency than in the primary response (7/77 GC tracks going from GC to FM in **Figures 1B** compared to 7/15 in **Figure 6B,** see also **Movies S1 with S6**). However, secondary T_{fh} cells located in the GC and FM had similar motility parameters (**Figure 6C and D).** Even more strikingly, activated memory KD OT2 T cells were observed to crawl between the cells lining the floor of the SCS to enter the lumen where they became rounded, and to detach and be carried away in the

lymphatic flow (**Figures 6E and F,** and **Movie S7**). We also observed activated memory KD OT2 cells arriving in the follicle via the lymphatics, presumably from an "upstream" follicle. In fact, when we optically marked secondary T_{fh} cells in the GC and reimaged the next day, >97% of the photoconverted cells had left the GC and relocalised to the FM in the original photoconverted follicle, or migrated to the FM of neighbouring and distant follicles (**Figures 6G and H,** and **Movie S9**). This data contrasts with the migration pattern of primary T_{fh} cells (**Figures 1A and B,** and **Movie S1**). Thus, T_{fh} cells in the secondary response are not confined to the GC and instead are able to migrate in and out of the follicle via the SCS.

Secondary T_{fh} cells in the FM and GC are molecularly heterogeneous

To investigate the differences in the migratory behaviour between primary and secondary T_{fh} cells we first examined surface expression of CCR7 and CXCR5 by optically marked cells in the FM and GC (**Figure 7A**). These analyses showed that unlike the primary response, secondary T_{fh} cells expressed similar levels of these chemokine receptors irrespective of their microanatomical compartment of origin. Both groups of secondary T_{fh} cells expressed high levels of *Bcl6* (**Figure 7B**). However, there were significant changes in the expression pattern of *Ccr7, Cxcr5, Gpr183* and *S1pr2* (**Figure 7C**). In particular, differences in expression levels that arose in the primary response were abolished in secondary T_{fh} cells. For example, selective downmodulation of *Gpr183* by primary GC T_{fh} was not observed in secondary the response where both FM and GC T_{fh} cells maintained high levels of this gene. This suggests that EBI2 was not involved in GC positioning of secondary T_{fh} cells and consistent with this EBI2-deficient KD OT2 T cells were able to generate secondary T_{fh} cells and colonise the GC upon rechallenge with the same efficiency as wildtype B cells (data not shown). Furthermore, selective induction of the regulator of G-protein signaling family member *Rgs16* (Estes et al., 2004) in primary GC T_{fh} cells was also absent in the secondary response (**Figure 7D**). These data suggest that the differences in migratory behaviour of T_{fh} cells in the primary and secondary response result from loss of differential chemokine receptor expression and sensitivity to global positioning signals by secondary T_{fh} cells in the GC and FM.

The free exchange of secondary T_{fh} cells between the FM and GC raised the possibility that, unlike the situation in the primary response, these are no longer molecularly distinct cell populations. This was also suggested by their similar gene expression profiles (**Figure 7E**). To explore this further, we analysed the 25 gene × 126 cell matrix from secondary T_{fh} cells by NMF and found that while the data could be stably decomposed into 2 clusters (k = 2, cophenetic correlation coefficient = 0.9654, **Figure S6**), these clusters did not segregate according to microanatomical location (**Figure 7F**). Indeed, the existence of the two factorised subpopulations was only apparent after reorganisation of the cells based on their metagene expression levels (**Figure 7G**). Thus, individual secondary T_{fh} cells from the FM and GC overlap in expression of metagenes S1 and S2 and were only separated by a Euclidean distance of 0.04 (**Figure 7H**). Intriguingly, vector analysis showed the major unique contributors to metagene S2 were *Bcl6* and *Pdcd1* (**Figure 7I**). Therefore, NMF analysis points to the presence of two molecular subpopulations that exist heterogeneously within both the FM and GC, rather than a homogeneous secondary Tfh cell population as would be inferred from the FACS (**Figure 7A**) and volcano plot (**Figure 7C**). Finally, we also combined the single cell gene expression data from primary and secondary responses and performed NMF analysis on all four groups (**Figure S7**). This confirmed the previous analyses and reproducibly identified primary GC T_{fh} cells as being molecularly distinct from secondary T_{fh} and primary FM T_{fh} cells. In addition, secondary T_{fh} cells from the FM and GC could not be resolved from each other even when model conditions were relaxed to allow for multiple clusters (rank k = 2-5).

DISCUSSION

The origin and fate of T_{fh} cells has been intensely studied since their first description 14 years ago (Breitfeld et al., 2000; Schaerli et al., 2000). While mice engineered to report BCL6 (Kitano et al., 2011; Liu et al., 2012) and IL-21 (Luthje et al., 2012) expression have provided powerful tools to analyse T_{fh} cells, their usefulness have been limited by T_{fh} cell heterogeneity and plasticity (Cannons et al., 2013). In this regard, the development of methods for the optical marking and tracking of cells based on their microanatomical location have created further opportunities for

more precise delineation of T_{fh} cell dynamics and the molecular cues that underpin their behaviour. Here we have used optical marking by TPP to link T_{fh} cell location to their behaviour, phenotype and gene expression. Our studies show remarkable differences in the migration pattern and single cell gene expression signatures between primary and secondary T_{fh} cells. In addition, we report a subpopulation of "follicular memory T cells" that reside in the follicle where they scan SCS macrophages to initiate the secondary immune response upon antigen re-exposure. This temporospatial dissection of T_{fh} cell dynamics offers multiple new insights into regulation of GC responses in naïve and antigen-experienced animals.

Imaging of primary T_{fh} cells at the peak of the GC response revealed clear spatial segregation in the FM and GC compartments. This confinement was confirmed by TPP and discontinuous cell tracking 24 hours later, which showed retention of the majority of photoconverted GC T_{fh} cells in the original GC and follicle. Furthermore, NMF analysis of single cell gene expression signatures of FM and GC T_{fh} cells support the notion that they represent molecularly distinct cell populations. Thus, we conclude that the primary GC is a closed structure designed to partition responding GC B cells and restrict their access to $CD4^+$ T cell help. At face value, these data contrasts with the findings of Shulman et al. who concluded that the GC is an open structure designed to broaden the diversity of the available $CD4^+$ T cell help (Shulman et al., 2013). However, the preliminary experiments in their paper only examined polychromatic responses in naïve animals that demonstrated initial colonisation by multiple clones of red, green or cyan T cells with the same TCR specificity and not interfollicular exchange as claimed. Furthermore, their subsequent experiments involved prime-boost immunisation protocols that involved repeated exposure to antigen. This is a critical point of difference as they do not show any equivalent photoactivation data from naïve responses (Shulman et al., 2013). Hence, their data is more consistent with our memory responses. In fact, we not only observed the migration of T_{fh} cells out of the GC in the secondary response, but also their remarkable transport in the lymphatic flow of the SCS. This novel passive transport mechanism whereby cells "surf" the lymph appears to be an efficient and

rapid mechanism for dissemination of cells that bypasses the need to traverse multiple anatomical compartments across disparate chemokine gradients. Regardless, it will be interesting to determine what role factors enriched in lymph such as S1P play in driving secondary T_{fh} cells to enter and leave the follicle.

Why are T_{fh} cell dynamics so fundamentally different in naïve and immune animals? Initially, GC B cells must pass stringent affinity and specificity checkpoints to ensure only high-affinity non-self-reactive cells are selected. Therefore, restricting primary T_{fh} cells with the greatest helper capacity to the GC may serve to direct help to cognate B cells and avoid the activation of bystander B cells in the follicle. Accordingly, expression of the genes encoding the B helper cytokines IL-21 and IL-4 were restricted to primary GC T_{fh} cells. In the secondary response, memory B cells have already passed these checkpoints and therefore have less stringent activation thresholds. Correspondingly, secondary T_{fh} do not express the same high level of *Il21* and *Il4* transcripts as primary GC T_{fh} cells. Furthermore, memory B cells are widely distributed in persistent GC remnants within the follicle (Dogan et al., 2009; Talay et al., 2012) and extrafollicular sites including the bone marrow (Dogan et al., 2009; Paramithiotis and Cooper, 1997), tonsillar mucosal epithelium (Liu et al., 1995) and splenic marginal zone (Liu et al., 1988). Therefore, protective secondary antibody responses may depend on the rapid extrafollicular export of secondary T_{fh} cells to these sites. Thus, unlike primary responses where it takes 7 days or more for T_{fh} cells to mature, the stereotypic expansion of $CXCR5^{hi}PD\text{-}1^{hi}$ cell with a "mature" T_{fh} cell phenotype that peaks by day 3 in our system may be a part of a pre-wired memory program (Hale et al., 2013). Nevertheless, some memory B cells do enter GCs (Dogan et al., 2009; Pape et al., 2011) and T_{fh} cells are still required in this location in the secondary response. In this respect, it is notable that the NMF analysis of single cell gene expression by secondary T_{fh} cells showed that there was a hidden subpopulation of cells with high expression of *Bcl6* and *Pdcd1* that may be destined to later colonise and persist in secondary GCs. Thus, follicular memory T cells also appear to bifurcate into two responding populations upon

rechallenge. However, at the peak of the secondary T_{fh} response these responding cells are equally likely to be in the FM or GC.

What are the molecular signals that guide T_{fh} cells as they navigate around the lymph node in the course of the immune response? It was recently reported that T_{fh} cells inside GCs expressed high levels of SIPR2, which acts to repel them from the S1P-rich lymph in the SCS and promote their retention in the GC (Moriyama et al., 2014). While *S1pr2* was also upregulated in our single cell gene expression analysis by primary GC T_{fh} cells, there were more striking changes in *Gpr183* gene and EBI2 protein expression levels. Moreover, gene function analysis using retroviral transduction and knockout mice confirmed a role for EBI2 in primary GC localisation. These data also closely parallel the role of EBI2 in the positioning of GC B cells (Gatto et al., 2009; Pereira et al., 2009). Conspicuously, there was no differential expression of a number of chemokine receptors including *Cxcr5, Ccr7, S1pr2* and *Gpr183* in secondary T_{fh} cells located in the FM and GC, and this may explain the lack of spatial confinement upon antigen recall. Accordingly, we did not detect a defect in GC localisation by EBI2-deficient KD OT2 T cells in secondary responses. Furthermore, *Rgs16* was induced in primary but not secondary GC T_{fh} cells, suggesting an additional layer of control in chemokine receptor signaling allows the cells to integrate the changes in expression of these and possibly other chemokine receptors to determine their global positioning.

Our finding that follicular memory T cells are located in the periphery of the draining lymph node is reminiscent of the CXCR3-dependent positioning of memory $CD8^+$ T cells in this location (Kastenmuller et al., 2013). This positioning of follicular memory T cells at the lymph-tissue interface may facilitate quick and efficient surveillance of SCS macrophages which act as "fly paper" (Junt et al., 2007) to capture lymph-borne antigens (Carrasco and Batista, 2007; Junt et al., 2007; Phan et al., 2007; Roozendaal et al., 2009), particularly the antigen-antibody immune complexes that are generated upon secondary exposure (Phan et al., 2007; Roozendaal et al., 2009). While SCS macrophages are slow to phagocytose (Phan et al., 2009), they are nevertheless still capable of processing and presenting protein antigen to $CD8^+$ T cells (Chtanova et al., 2009;

Hickman et al., 2008), and lipid antigens to iNKT cells (Barral et al., 2010). Thus, the finding that follicular memory T cells are activated to proliferate in the subcapsular region also resolves the question of how and where the secondary antibody response is initiated. Interestingly, memory B cells were recently shown to induce rapid BCL6 upregulation by "memory T_{fh} cells" in the spleen in the absence of dendritic cells (Ise et al., 2014). However, these experiments examined recall responses in the spleen of naïve recipient mice following adoptive transfer of FACS-sorted "memory T_{fh} cells". In contrast, we examined the *in situ* recall responses made by persistent antigen-specific cells in the lymph node of immune animals without any *ex vivo* manipulation. It should also be noted that other groups have been able to generate robust memory responses in naïve recipient mice without the need for co-transfer of memory B cells (Luthje et al., 2012; Weber et al., 2012). Hence, while memory B cells may support secondary T_{fh} responses at the T-B border under some circumstances, it is likely that local responses in draining lymph nodes can also be generated in the subcapsular region. Nevertheless, this temporospatial organisation of memory responses bypasses the need for shuttling of primary T_{fh} cells from the T cell zone to the T-B border and finally into the follicle, and ensures rapid intrafollicular generation of secondary T_{fh} cells. Taken together, these data show that T_{fh} cell heterogeneity and complexity can be resolved by temporospatial dissection of their behaviour and the molecular cues that guide this behaviour. It is hoped that future studies using non-linear optical marking and single cell genomics will reveal further insights into T_{fh} cell biology and thereby provide cellular and molecular targets that could be manipulated to augment or dampen the antibody response to treat human diseases.

EXPERIMENTAL PROCEDURES

Animals

Transgenic and knockout mice used are described in **Supplemental Experimental Procedures**. Animal experiments were approved by the Garvan Institute of Medical Research/St Vincent's Hospital Animal Ethics Committee.

Immunisations, antigen trafficking and *in vivo* fiducial labeling

2.5×10^5 $CD4^+V_\alpha2^+$ KD OT2 were enriched by MACS negative depletion and adoptively transferred into age and sex-matched 6-10 week old SAP-deficient recipient mice and immunised with 20μg of OVA in Sigma Adjuvant System (SAS, Sigma). For memory responses, immunised mice were rested for 28-95 days and rechallenged with 40μg of OVA in SAS. In some experiments, we also co-transferred 2.5×10^5 HEL^+ SW_{HEL} tdTomato B cells and $V_\alpha2^+$ $CD4^+$ KD OT2 into SAP-deficient recipients and immunised with 20μg HEL-OVA. To track antigen trafficking , OVA-PE and HEL-PE was injected subcutaneously in mice immunised >28 days earlier. To label the B cell follicular stroma *in vivo*, we injected anti-CD157 subcutaneously the day before imaging (Phan et al., 2007). To label the GC *in vivo*, we injected anti-CD157 subcutaneoulsy 3-4 days before imaging. See **Fig. S3** and **Supplemental Experimental Procedure** for detailed description and validation of this labeling strategy. In some experiments, we also transferred CFP B cells as an additional fiducial label.

Retroviral transduction of primary T cells

See **Supplemental Experimental Procedures**.

Two-photon microscopy and two-photon photoconversion

See **Supplemental Experimental Procedures**.

Image analysis and cell tracking

See **Supplemental Experimental Procedures**.

FACS analysis and single cell FACS sorting

See **Supplemental Experimental Procedures**.

Single cell RT-qPCR

See **Supplemental Experimental Procedures**.

Pre-processing of single cell gene expression data

See **Supplemental Experimental Procedures**.

Gene expression analysis by NMF

See **Supplemental Experimental Procedures**.

Statistical analysis

See **Supplemental Experimental Procedures**.

ACKNOWLEDGMENTS

We thank T. Okada, J. Cyster, I. Grigorova and D. Butt for helpful discussions, and A. Basten and C. Sundling for comments on the manuscript. We thank P. Schwartzberg for SAP KO mice. We also thank J-H. Cho for the primary T cell retroviral transduction protocol, N. Anders from the Small Animal Imaging Facility, R. Solomon and D. Snowden from the MLC Flow Cytometry Facility and P. Bitter from the ACRF Facility. D.S. is supported by an NHMRC Post-graduate Scholarship, I.M. and H.R.H. by an Australian Post-graduate Award, S.G.T., A.D.K. and R.B. by Research Fellowships from the NHMRC and T.C. and T.G.P. by Career Development Fellowships from the NHMRC. This work was funded by Peter and Val Duncan, NHMRC Project Grants 1004632 (T.G.P.), 1062332 (T.C. and T.G.P.) and NHMRC Program Grant 1016953 (R.B. and S.G.T.).

REFERENCES

Allen, C.D., Okada, T., and Cyster, J.G. (2007). Germinal-center organization and cellular dynamics. Immunity *27*, 190-202.

Ansel, K.M., McHeyzer-Williams, L.J., Ngo, V.N., McHeyzer-Williams, M.G., and Cyster, J.G. (1999). In vivo-activated CD4 T cells upregulate CXC chemokine receptor 5 and reprogram their response to lymphoid chemokines. J Exp Med *190*, 1123-1134.

Barral, P., Polzella, P., Bruckbauer, A., van Rooijen, N., Besra, G.S., Cerundolo, V., and Batista, F.D. (2010). CD169(+) macrophages present lipid antigens to mediate early activation of iNKT cells in lymph nodes. Nat Immunol *11*, 303-312.

Baumjohann, D., Okada, T., and Ansel, K.M. (2011). Cutting Edge: Distinct waves of BCL6 expression during T follicular helper cell development. J Immunol *187*, 2089-2092.

Breitfeld, D., Ohl, L., Kremmer, E., Ellwart, J., Sallusto, F., Lipp, M., and Forster, R. (2000). Follicular B helper T cells express CXC chemokine receptor 5, localize to B cell follicles, and support immunoglobulin production. J Exp Med *192*, 1545-1552.

Brunet, J.P., Tamayo, P., Golub, T.R., and Mesirov, J.P. (2004). Metagenes and molecular pattern discovery using matrix factorization. Proc Natl Acad Sci U S A *101*, 4164-4169.

Cannons, J.L., Lu, K.T., and Schwartzberg, P.L. (2013). T follicular helper cell diversity and plasticity. Trends Immunol *34*, 200-207.

Carrasco, Y.R., and Batista, F.D. (2007). B cells acquire particulate antigen in a macrophage-rich area at the boundary between the follicle and the subcapsular sinus of the lymph node. Immunity *27*, 160-171.

Chtanova, T., Hampton, H.R., Waterhouse, L.A., Wood, K., Tomura, M., Miwa, Y., Mackay, C.R., Brink, R., and Phan, T.G. (2014). Real-time interactive two-photon photoconversion of recirculating lymphocytes for discontinuous cell tracking in live adult mice. J Biophotonics *7*, 425-433.

Chtanova, T., Han, S.J., Schaeffer, M., van Dooren, G.G., Herzmark, P., Striepen, B., and Robey, E.A. (2009). Dynamics of T cell, antigen-presenting cell, and pathogen interactions during recall responses in the lymph node. Immunity *31*, 342-355.

Chtanova, T., Tangye, S.G., Newton, R., Frank, N., Hodge, M.R., Rolph, M.S., and Mackay, C.R. (2004). T follicular helper cells express a distinctive transcriptional profile, reflecting their role as non-Th1/Th2 effector cells that provide help for B cells. J Immunol *173*, 68-78.

Crotty, S. (2011). Follicular helper CD4 T cells (TFH). Annu Rev Immunol *29*, 621-663.

Czar, M.J., Kersh, E.N., Mijares, L.A., Lanier, G., Lewis, J., Yap, G., Chen, A., Sher, A., Duckett, C.S., Ahmed, R., and Schwartzberg, P.L. (2001). Altered lymphocyte responses and cytokine production in mice deficient in the X-linked lymphoproliferative disease gene SH2D1A/DSHP/SAP. Proc Natl Acad Sci U S A *98*, 7449-7454.

Dogan, I., Bertocci, B., Vilmont, V., Delbos, F., Megret, J., Storck, S., Reynaud, C.A., and Weill, J.C. (2009). Multiple layers of B cell memory with different effector functions. Nat Immunol *10*, 1292-1299.

Estes, J.D., Thacker, T.C., Hampton, D.L., Kell, S.A., Keele, B.F., Palenske, E.A., Druey, K.M., and Burton, G.F. (2004). Follicular dendritic cell regulation of CXCR4-mediated germinal center CD4 T cell migration. J Immunol *173*, 6169-6178.

Garside, P., Ingulli, E., Merica, R.R., Johnson, J.G., Noelle, R.J., and Jenkins, M.K. (1998). Visualization of specific B and T lymphocyte interactions in the lymph node. Science *281*, 96-99.

Gatto, D., Paus, D., Basten, A., Mackay, C.R., and Brink, R. (2009). Guidance of B cells by the orphan G protein-coupled receptor EBI2 shapes humoral immune responses. Immunity *31*, 259-269.

Hale, J.S., Youngblood, B., Latner, D.R., Mohammed, A.U., Ye, L., Akondy, R.S., Wu, T., Iyer, S.S., and Ahmed, R. (2013). Distinct memory CD4+ T cells with commitment to T follicular helper- and T helper 1-cell lineages are generated after acute viral infection. Immunity *38*, 805-817.

Hardie, D.L., Johnson, G.D., Khan, M., and MacLennan, I.C. (1993). Quantitative analysis of molecules which distinguish functional compartments within germinal centers. Eur J Immunol *23*, 997-1004.

Haynes, N.M., Allen, C.D., Lesley, R., Ansel, K.M., Killeen, N., and Cyster, J.G. (2007). Role of CXCR5 and CCR7 in follicular Th cell positioning and appearance of a programmed cell death gene-1high germinal center-associated subpopulation. J Immunol *179*, 5099-5108.

Hickman, H.D., Takeda, K., Skon, C.N., Murray, F.R., Hensley, S.E., Loomis, J., Barber, G.N., Bennink, J.R., and Yewdell, J.W. (2008). Direct priming of antiviral CD8+ T cells in the peripheral interfollicular region of lymph nodes. Nat Immunol *9*, 155-165.

Ise, W., Inoue, T., McLachlan, J.B., Kometani, K., Kubo, M., Okada, T., and Kurosaki, T. (2014). Memory B cells contribute to rapid Bcl6 expression by memory follicular helper T cells. Proc Natl Acad Sci U S A *111*, 11792-11797.

Johnston, R.J., Poholek, A.C., DiToro, D., Yusuf, I., Eto, D., Barnett, B., Dent, A.L., Craft, J., and Crotty, S. (2009). Bcl6 and Blimp-1 are reciprocal and antagonistic regulators of T follicular helper cell differentiation. Science *325*, 1006-1010.

Junt, T., Moseman, E.A., Iannacone, M., Massberg, S., Lang, P.A., Boes, M., Fink, K., Henrickson, S.E., Shayakhmetov, D.M., Di Paolo, N.C., *et al.* (2007). Subcapsular sinus macrophages in lymph nodes clear lymph-borne viruses and present them to antiviral B cells. Nature *450*, 110-114.

Kastenmuller, W., Brandes, M., Wang, Z., Herz, J., Egen, J.G., and Germain, R.N. (2013). Peripheral prepositioning and local CXCL9 chemokine-mediated guidance orchestrate rapid memory CD8+ T cell responses in the lymph node. Immunity *38*, 502-513.

Kerfoot, S.M., Yaari, G., Patel, J.R., Johnson, K.L., Gonzalez, D.G., Kleinstein, S.H., and Haberman, A.M. (2011). Germinal center B cell and T follicular helper cell development initiates in the interfollicular zone. Immunity *34*, 947-960.

Kitano, M., Moriyama, S., Ando, Y., Hikida, M., Mori, Y., Kurosaki, T., and Okada, T. (2011). Bcl6 protein expression shapes pre-germinal center B cell dynamics and follicular helper T cell heterogeneity. Immunity *34*, 961-972.

Liu, X., Yan, X., Zhong, B., Nurieva, R.I., Wang, A., Wang, X., Martin-Orozco, N., Wang, Y., Chang, S.H., Esplugues, E., *et al.* (2012). Bcl6 expression specifies the T follicular helper cell program in vivo. J Exp Med *209*, 1841-1852, S1841-1824.

Liu, Y.J., Barthelemy, C., de Bouteiller, O., Arpin, C., Durand, I., and Banchereau, J. (1995). Memory B cells from human tonsils colonize mucosal epithelium and directly present antigen to T cells by rapid up-regulation of B7-1 and B7-2. Immunity *2*, 239-248.

Liu, Y.J., Oldfield, S., and MacLennan, I.C. (1988). Memory B cells in T cell-dependent antibody responses colonize the splenic marginal zones. Eur J Immunol *18*, 355-362.

Luthje, K., Kallies, A., Shimohakamada, Y., Belz, G.T., Light, A., Tarlinton, D.M., and Nutt, S.L. (2012). The development and fate of follicular helper T cells defined by an IL-21 reporter mouse. Nat Immunol *13*, 491-498.

MacLennan, I.C. (1994). Germinal centers. Annu Rev Immunol *12*, 117-139.

Moriyama, S., Takahashi, N., Green, J.A., Hori, S., Kubo, M., Cyster, J.G., and Okada, T. (2014). Sphingosine-1-phosphate receptor 2 is critical for follicular helper T cell retention in germinal centers. J Exp Med *211*, 1297-1305.

Nurieva, R.I., Chung, Y., Martinez, G.J., Yang, X.O., Tanaka, S., Matskevitch, T.D., Wang, Y.H., and Dong, C. (2009). Bcl6 mediates the development of T follicular helper cells. Science *325*, 1001-1005.

Okada, T., Miller, M.J., Parker, I., Krummel, M.F., Neighbors, M., Hartley, S.B., O'Garra, A., Cahalan, M.D., and Cyster, J.G. (2005). Antigen-engaged B cells undergo chemotaxis toward the T zone and form motile conjugates with helper T cells. PLoS Biol *3*, e150.

Pape, K.A., Taylor, J.J., Maul, R.W., Gearhart, P.J., and Jenkins, M.K. (2011). Different B cell populations mediate early and late memory during an endogenous immune response. Science *331*, 1203-1207.

Paramithiotis, E., and Cooper, M.D. (1997). Memory B lymphocytes migrate to bone marrow in humans. Proc Natl Acad Sci U S A *94*, 208-212.

Pereira, J.P., Kelly, L.M., Xu, Y., and Cyster, J.G. (2009). EBI2 mediates B cell segregation between the outer and centre follicle. Nature *460*, 1122-1126.

Phan, T.G., Green, J.A., Gray, E.E., Xu, Y., and Cyster, J.G. (2009). Immune complex relay by subcapsular sinus macrophages and noncognate B cells drives antibody affinity maturation. Nat Immunol *10*, 786-793.

Phan, T.G., Grigorova, I., Okada, T., and Cyster, J.G. (2007). Subcapsular encounter and complement-dependent transport of immune complexes by lymph node B cells. Nat Immunol *8*, 992-1000.

Plotkin, S.A. (2008). Vaccines: correlates of vaccine-induced immunity. Clin Infect Dis *47*, 401-409.

Rasheed, A.U., Rahn, H.P., Sallusto, F., Lipp, M., and Muller, G. (2006). Follicular B helper T cell activity is confined to CXCR5(hi)ICOS(hi) CD4 T cells and is independent of CD57 expression. Eur J Immunol *36*, 1892-1903.

Roozendaal, R., Mempel, T.R., Pitcher, L.A., Gonzalez, S.F., Verschoor, A., Mebius, R.E., von Andrian, U.H., and Carroll, M.C. (2009). Conduits mediate transport of low-molecular-weight antigen to lymph node follicles. Immunity *30*, 264-276.

Schaerli, P., Loetscher, P., and Moser, B. (2001). Cutting edge: induction of follicular homing precedes effector Th cell development. J Immunol *167*, 6082-6086.

Schaerli, P., Willimann, K., Lang, A.B., Lipp, M., Loetscher, P., and Moser, B. (2000). CXC chemokine receptor 5 expression defines follicular homing T cells with B cell helper function. J Exp Med *192*, 1553-1562.

Shulman, Z., Gitlin, A.D., Targ, S., Jankovic, M., Pasqual, G., Nussenzweig, M.C., and Victora, G.D. (2013). T follicular helper cell dynamics in germinal centers. Science *341*, 673-677.

Talay, O., Yan, D., Brightbill, H.D., Straney, E.E., Zhou, M., Ladi, E., Lee, W.P., Egen, J.G., Austin, C.D., Xu, M., and Wu, L.C. (2012). IgE(+) memory B cells and plasma cells generated through a germinal-center pathway. Nat Immunol *13*, 396-404.

Tangye, S.G., Ma, C.S., Brink, R., and Deenick, E.K. (2013). The good, the bad and the ugly - TFH cells in human health and disease. Nat Rev Immunol *13*, 412-426.

Victora, G.D., and Nussenzweig, M.C. (2012). Germinal centers. Annu Rev Immunol *30*, 429-457.

Victora, G.D., Schwickert, T.A., Fooksman, D.R., Kamphorst, A.O., Meyer-Hermann, M., Dustin, M.L., and Nussenzweig, M.C. (2010). Germinal center dynamics revealed by multiphoton microscopy with a photoactivatable fluorescent reporter. Cell *143*, 592-605.

Weber, J.P., Fuhrmann, F., and Hutloff, A. (2012). T-follicular helper cells survive as long-term memory cells. Eur J Immunol *42*, 1981-1988.

Yu, D., Rao, S., Tsai, L.M., Lee, S.K., He, Y., Sutcliffe, E.L., Srivastava, M., Linterman, M., Zheng, L., Simpson, N., *et al.* (2009). The transcriptional repressor Bcl-6 directs T follicular helper cell lineage commitment. Immunity *31*, 457-468.

FIGURE LEGENDS

Figure 1. Spatial segregation of primary T_{fh} cells into FM and GC compartments. (**A**) Maximal intensity projection (398×390×75μm) of follicle on day 7 showing primary T_{fh} cells (green) localise in the GC (magenta) and FM. Capsule is blue from SHG. (**B**) Cell tracking analysis of (**A**) showing the spatial confinement of cells in the GC and FM. See also **Movie S1**. (**C**) Distribution of instantaneous velocities of primary FM and GC T_{fh} cells. Arrows indicate median (7.8μm/min for GC, and 8.5μm/min for FM T_{fh} cells). (**D**) Confinement index of primary GC and FM T_{fh} cells. (**E**) Retention of photoconverted GC T_{fh} cells (marked by red spheres) in the original follicle and GC (white) after 24 hours. Unphotoconverted T_{fh} cells are green; polyclonal B cells cyan and capsule blue from SHG. Yellow triangles indicate photoconverted cells that have migrated to the neighbouring GC. See also **Movie S2**. (**F**) Cropped 3D rendered volume of lymph node from (**E**) showing confinement of photoconverted red cells (marked by red spheres) to the GC and FM of the original follicle. (**G**) Comparison of the localisation of photoconverted GC T_{fh} cells to unphotoconverted T_{fh} cells. PC GC = cells in photoconverted GC; FM adj. to PC GC = cells in FM adjacent to the original PC GC; other follicle = cells that have migrated outside follicle containing PC GC. Representative data (**A-C, E and F**) and pooled data (**D and G**) is from at least 3 experiments.

Figure 2. Primary FM and GC T_{fh} cells are distinct cell populations. (**A**) Maximal intensity projection (332×332×99μm) of follicle immediately after TPP of GC T_{fh} cells on day 7. Dashed box indicates the targeted ROI in the GC (white); unphotoconverted KD OT2 cells (green); photoconverted KD OT2 (red); capsule SHG (blue). Note bleaching of the GC label from photoconversion. Multiple lymph nodes were photoconverted and pooled. FACS analysis shows expression of CXCR5 and PD-1 by photoconverted red KD OT2 and unphotoconverted green KD OT2 cells. (**B**) Maximal intensity projection (332×332×99μm) of follicle immediately after TPP of FM T_{fh} cells. Fluorescent labels same as in (**A**). Multiple lymph nodes were photoconverted and pooled. FACS analysis shows expression of CXCR5 and PD-1 by photoconverted red KD OT2 and

unphotoconverted green KD OT2 cells. (**C**) FACS data from (**A**) and (**B**) were overlaid to show overlapping expression of CXCR5 and PD-1 by endogenous (blue), FM (green) and GC T_{fh} cells (red). (**D**) Histograms of CCR7, CXCR5 and PD-1 expression by endogenous (blue), FM (green) and GC T_{fh} cells (red). Representative data from 3 experiments. KD OT2 cells in the FM (*n*=62) and GC (*n*=64) were optically marked by TPP and red cells FACS sorted for single cell RT-qPCR on day 7. (**E**) Volcano plot showing differentially expressed genes in primary FM compared to GC T_{fh} cells. Downregulated genes are red, upregulated genes green and non-differentially expressed genes blue. Intersecting lines indicate *p*-value of 0.05 and fold-change of 2. (**F**) Expression profile of two metagenes identified by NMF analysis across primary FM and GC T_{fh} cells (left panel), and across the samples re-ordered according to relative metagene expression (right panel). Red, metagene P1; blue, metagene P2. (**G**) Cluster analysis of primary FM and GC T_{fh} cells. Metagene P2 expression was plotted against metagene P1 expression for each cell. (**H**) Vector loadings of each gene to metagene P1 and P2. Single cell expression data is pooled from 2 identical independent experiments.

Figure 3. EBI2 promotes the spatial segregation of primary FM and GC T_{fh} cells. (**A**) Overlay histogram from FACS analysis for EBI2 expression by endogenous $CD4^+$ (blue), KD OT2 (green) and $CXCR5^{hi}PD\text{-}1^+$ KD OT2 T cells (red) on day 3, 7 and 14. (**B**) Plot of EBI2 expression relative to $B220^+$ B cells by endogenous $CD4^+$ (blue) and $CXCR5^{hi}PD\text{-}1^+$ KD OT2 T cells (red) from (**A**). (**C**) FACS plot of EBI2 and PD-1 expression by KD OT2 T cells from (**A**). (**D**) EBI2 expression by optically marked FM and GC T_{fh} cells on day 7. (**E**) Localisation OT2 T cells retrovirally transduced with either empty (left panel) or EBI2 (right panel) expression vector on day 7 after GFP^+ cells were sorted, adoptively transferred and immunised. (**F**) Quantification of the proportion of green T_{fh} cells that localise to the GC from (**E**). (**G**) Localisation of KD OT2 cells from wildtype (left panel) and EBI2-deficient (right panel) donors on day 7 after adoptive transfer and immunisation. (**H**) Quantification of the proportion of green T_{fh} cells that localise to the GC from

(**G**). Representative data (**A, C, D, E and G**) and pooled data (**B, F and H**) from three independent experiments is shown.

Figure 4. Follicular memory T cells cells localise to the outer follicle and scan SCS macrophages. (**A**) Maximal intensity projection (1992×1494×30µm) of immune lymph node on day 35 showing persistence of antigen-specific KD OT2 T cells (marked by green spheres) in the follicle (magenta). Collagen in capsule is blue, polyclonal CFP B cells are cyan. The number of cells inside and outside follicles for the whole tiled volume is shown. See also **Movie S3.** (**B**) Maximal intensity projection (2124×1274×30µm) of immune lymph node on day 30 showing persistence of antigen-specific KD OT2 T cells (marked by green spheres) in the proximity to $CD169^{+}$ SCS macrophages (magenta). Collagen in capsule is blue. See also **Movie S3.** (**C**) Rendered 212×212×99µm volume of draining lymph node 37 days after primary immunisation. Follicular memory T cells (green) localise in the periphery adjacent to SCS macrophages (CD169, magenta). Tracks of follicular memory T cells cells scanning SCS macrophages (red line) and migrating from the follicle up to the SCS macrophages (blue lines) are shown. See also **Movie S4**. (**D**) Residence time of follicular memory T cells in the follicle and subcapsular region. Individual tracks were segmented based on their proximity to SCS macrophages and the residence time as percentage of track duration calculated. (**E**) Median instantaneous velocity of follicular memory T cells when in the follicle (11.3 µm/min) and in proximity to SCS macrophages (4.0 µm/min) were calculated from track segments. (**F**) Arrest coefficient defined as percentage of time a cell slowed down to <3µm/min. (**G**) Motility coefficients for cells while distal (blue) and proximal to SCS macrophages (red). Data is pooled from 42 track segments from 26 individual cells tracked in 3 separate mice. (**H**) Time-lapse images showing follicular memory T cells (green) scanning SCS macrophages (magenta) for antigen. Colocalization channel between green and magenta is pseudo-coloured yellow. Time stamp is hh:mm:ss. See also **Movie S4**.

Figure 5. Follicular memory T cells are activated in the subcapsular region. (**A**) Comparison of antigen trapping of red HEL-PE control (left) and OVA-PE immune complexes (right) by SCS

macrophages (white) 4 hours after injection. Note the follicular memory T cells (green highlighted with yellow circle). (**B**) Quantification of amount of antigen trapping by counting red spots. (**C**) Redistribution of follicular memory T cells to the subcapsular region 4 hours after rechallenge with OVA-PE but not HEL-PE. (**D**) Mice were rechallenged with OVA and draining lymph node imaged 2 days later. Still frames show representative secondary T_{fh} cells in the subcapsular region (top) and inner follicle (bottom). See also **Movie S5**. (**E**) Cell shape index calculated for 56 cells in the subcapsular region and 98 cells in the inner follicle. (**F**) Arrest coefficient calculated for 67 cell tracks in the subcapsular region and 197 cell tracks in the inner follicle. (**G**) Examples of cells migrating on day 2 after rechallenge in relation to SCS macrophages. **(H)** Selected time-lapse images on day 2 after rechallenge showing a secondary T_{fh} cells dividing (white outline, inset) in contact with CD169-labeled SCS macrophages (red). Follicular stroma (magenta); capsule SHG (blue). See also **Movie S5**.

Figure 6. Secondary T_{fh} cells enter and leave the follicle via the lymphatics. (**A**) Maximal intensity projection (393×407×96µm) of follicle on day 5 after rechallenge showing secondary T_{fh} cells (green) localise in the GC (magenta) and FM. Capsule is blue from SHG. (**B**) Cell tracking analysis of (**A**) showing the spatial confinement of cells in the GC and FM. See also **Movie S6**. (**C**) Distribution of instantaneous velocities of secondary T_{fh} cells in the FM and GC. Arrows indicate median (5.8µm/min for GC and 7.6µm/min for FM). (**D**) Confinement index of secondary T_{fh} cells in the FM and GC. (**E**) Rendered 332×332×51µm volume showing secondary T_{fh} cells (green) entering (yellow tracks) and leaving the follicle (green tracks) via the SCS. Tracks of secondary T_{fh} cells migrating from the follicle to subcapsular region (red) and from the subcapsular region to the follicle (blue) are shown for comparison. See also **Movie S7**. (**F**) Instantaneous velocities of representative tracks from (**E**) showing changes in relation to their microanatomical location. Dashed line indicates threshold of 3µm/min. (**G**) Cropped mosaic tile image of lymph node showing dissemination of photoconverted GC T_{fh} cells (marked by red spheres) out of the original follicle after 24 hours. Unphotoconverted T_{fh} cells, green; polyclonal B cells, cyan; capsule, blue

from SHG. Inset shows raw image from single optical plane with 2 photoconverted cells (yellow; red arrows) located just beneath the capsule. See also **Movie S7**. (**H**) Comparison of the GC localisation of photoconverted to unphotoconverted secondary T_{fh} cells. PC GC = cells in photoconverted GC; FM adj. to PC GC = cells in FM adjacent to the original PC GC; other follicle = cells that have migrated outside follicle containing PC GC. Data is from at least 3 experiments.

Figure 7. Secondary T_{fh} cells from FM and GC share the same phenotype and gene expression patterns. Recipient mice were immunised and re-challenged 30 days later. Lymph nodes were harvested at the peak of the secondary response on day 5 post antigen-recall and cells in the FM and GC photoconverted for FACS analysis and single cell RT-qPCR. (**A**) Histograms of CCR7, CXCR5 and PD-1 expression by endogenous (blue), FM (green) and GC T_{fh} cells (red) from the secondary response. Representative data from 2 independent experiments. Relative single cell expression of (**B**) *Bcl6*, (**C**) *Ccr7*, *Cxcr5*, *Gpr183* and *S1pr2*, and (**D**) *Rgs16*. (**E**) Volcano plot comparing expression of 25 genes by secondary T_{fh} cells in the FM (n=64) and GC (n=64). (**F**) The expression of the two metagenes, S1 (red) and S2 (black), as identified by NMF, are not associated with localization of secondary Tfh cells to the FM (green) or GC (orange). (**G**) Re-ordering of the cells based on metagene expression reveals hidden clusters independent of their location. (**H**) Cluster analysis of secondary T_{fh} cells showing metagene expression by single cells and the Euclidean distance between the centroid of the cells from the FM and GC groups. (**I**) Vector contributions of each gene to metagene S1 and S2. Single cell data expression is pooled from 2 identical independent experiments.

Figure 1
Click here to download high resolution image

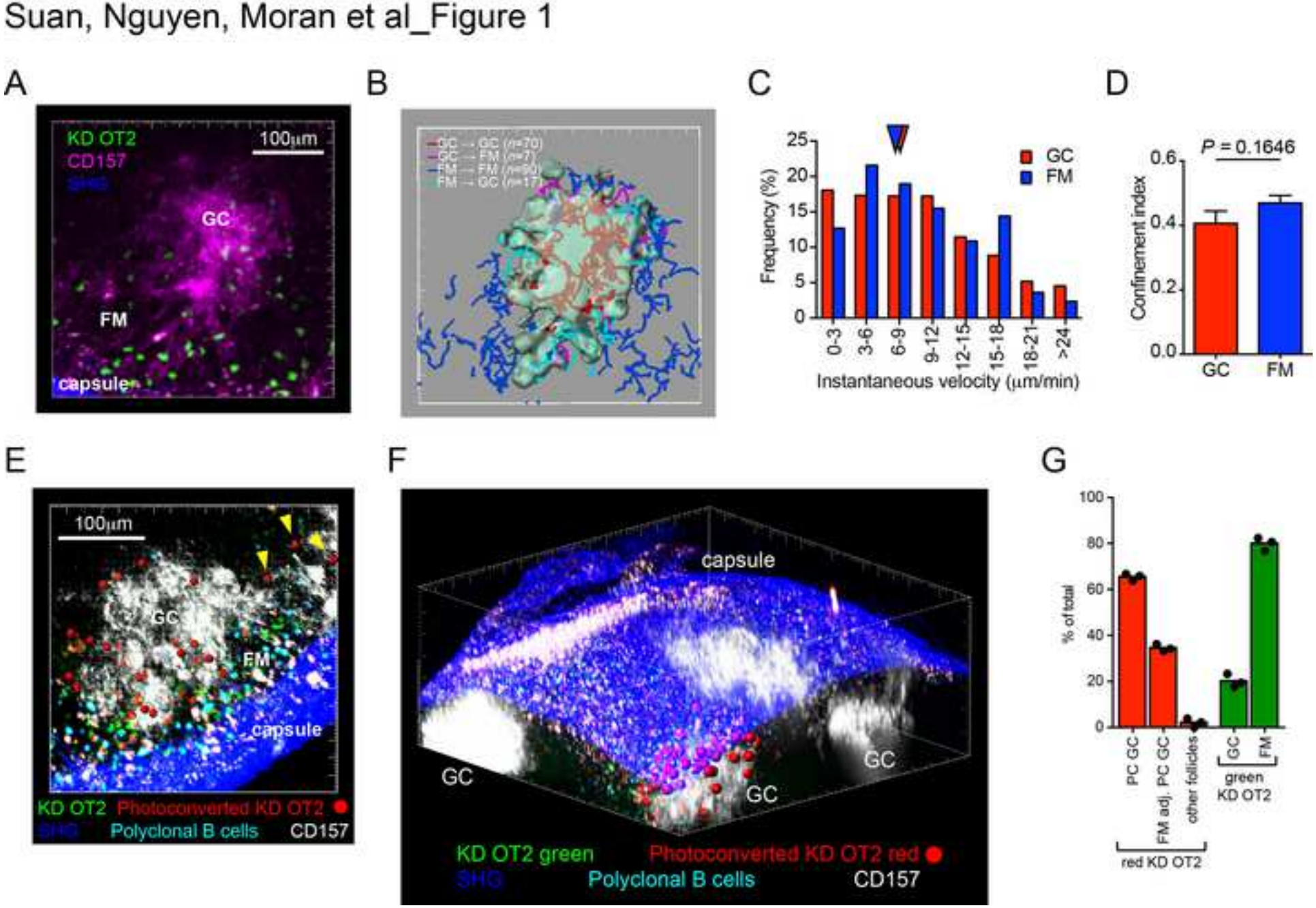

Figure 2
Click here to download high resolution image

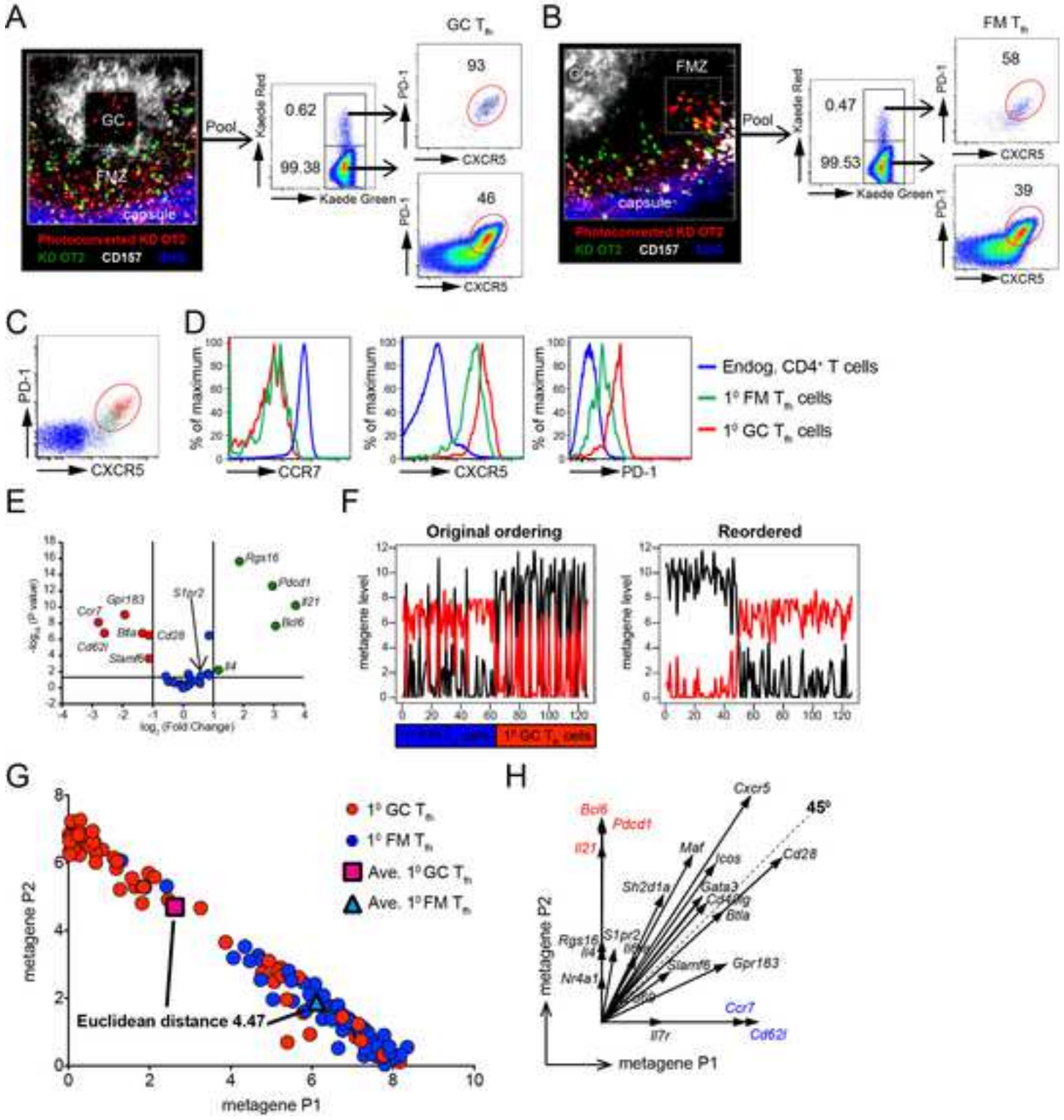

Figure 3
Click here to download high resolution image

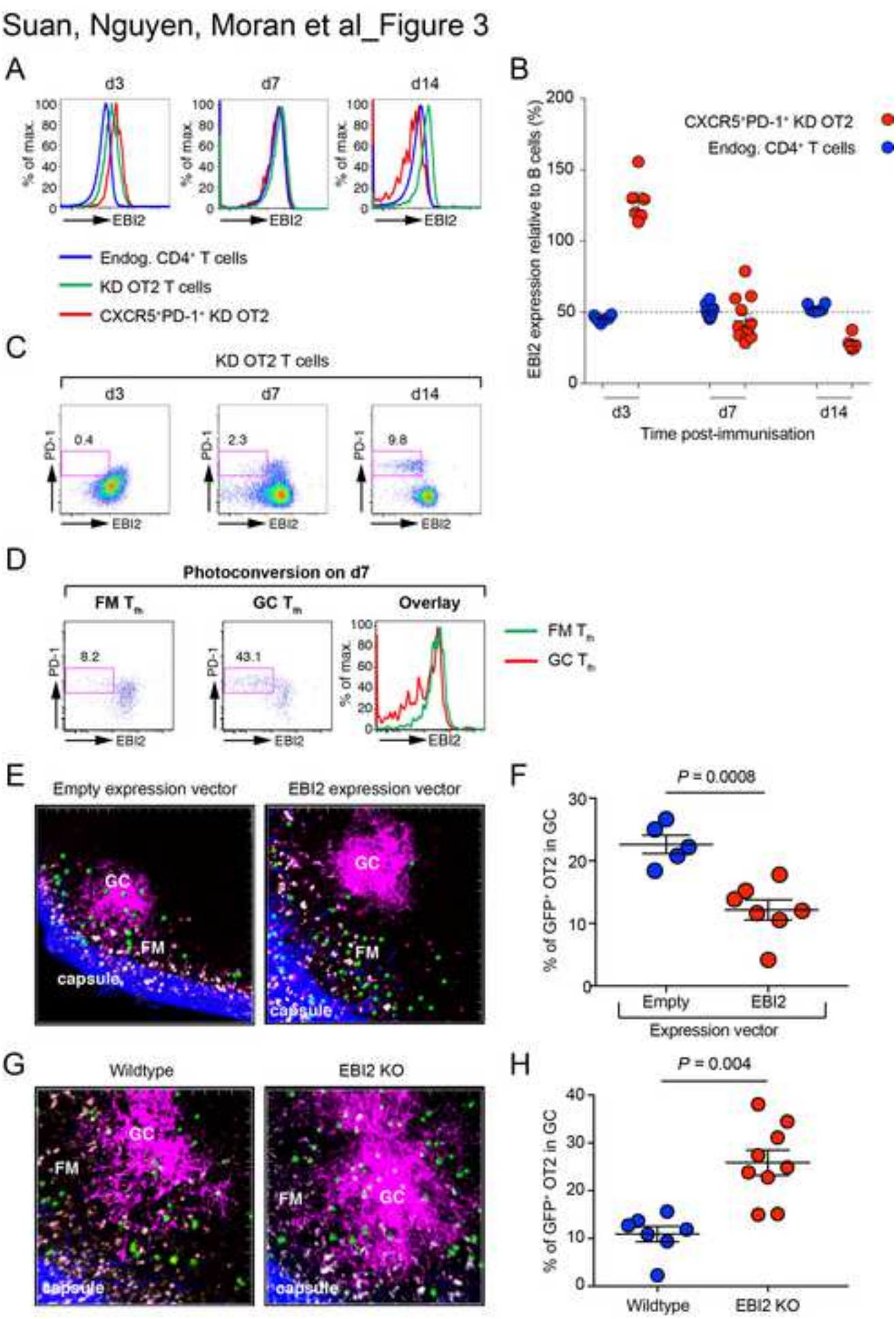

Figure 4
Click here to download high resolution image

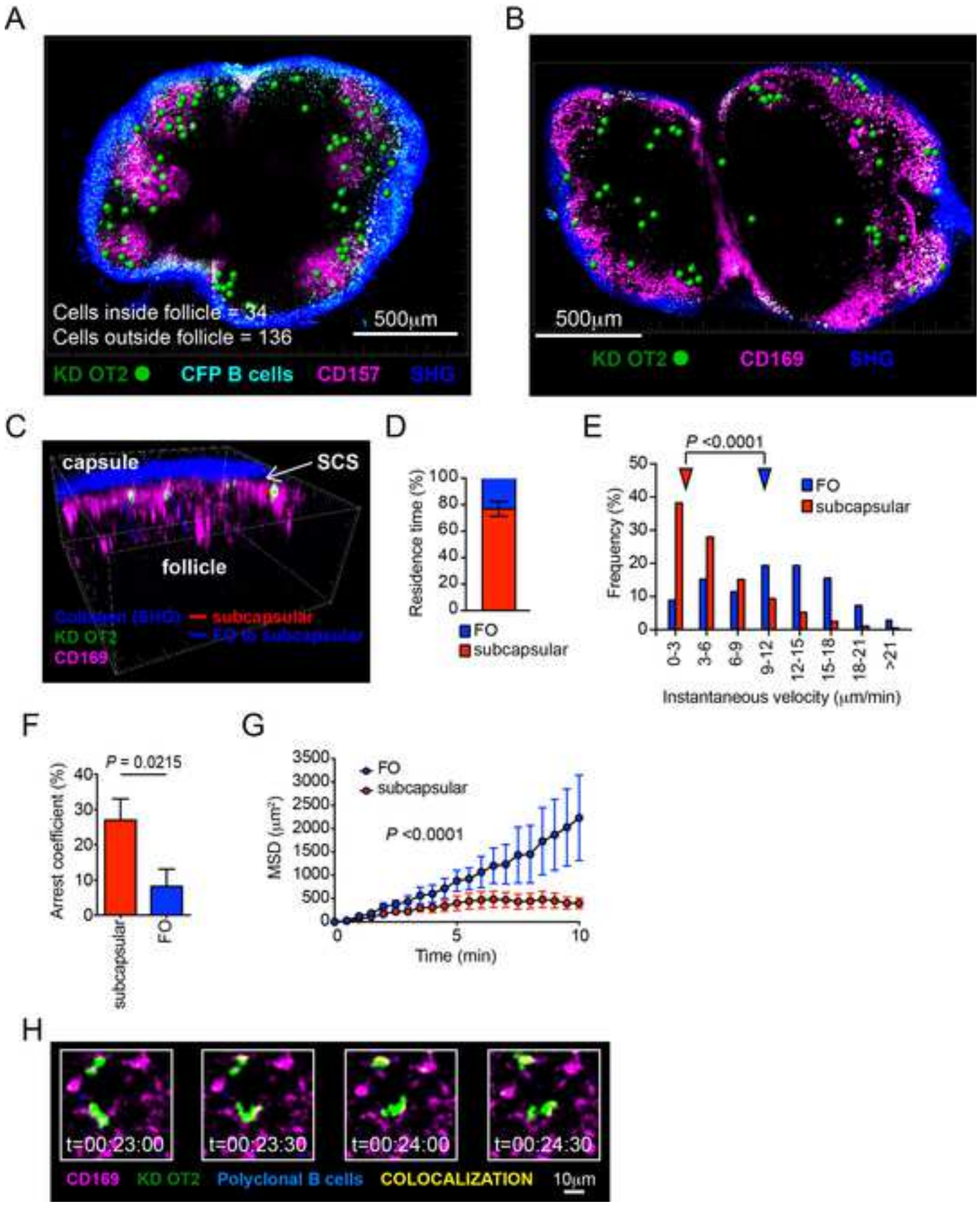

Figure 5
Click here to download high resolution image

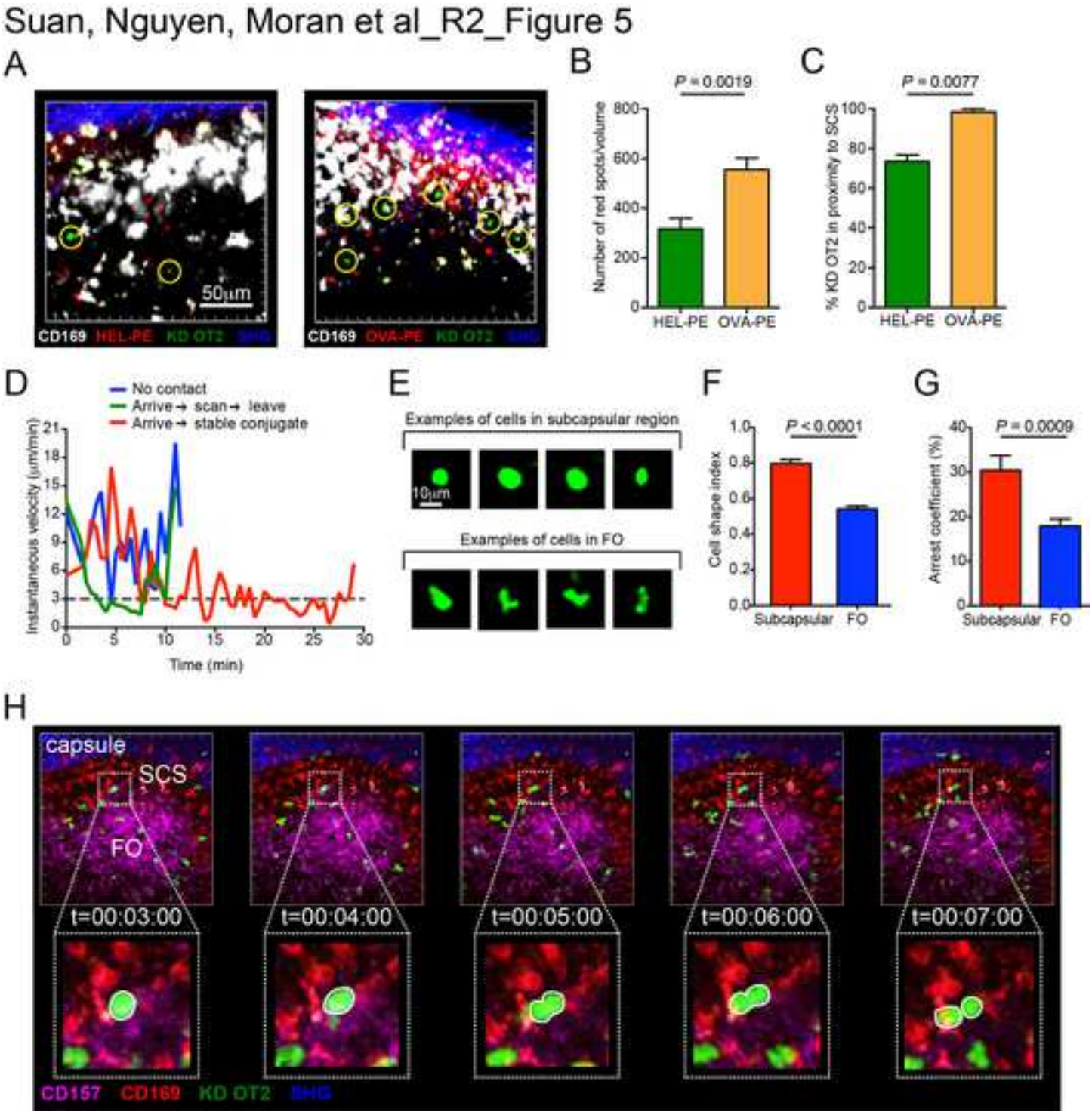

Figure 6

Click here to download high resolution image

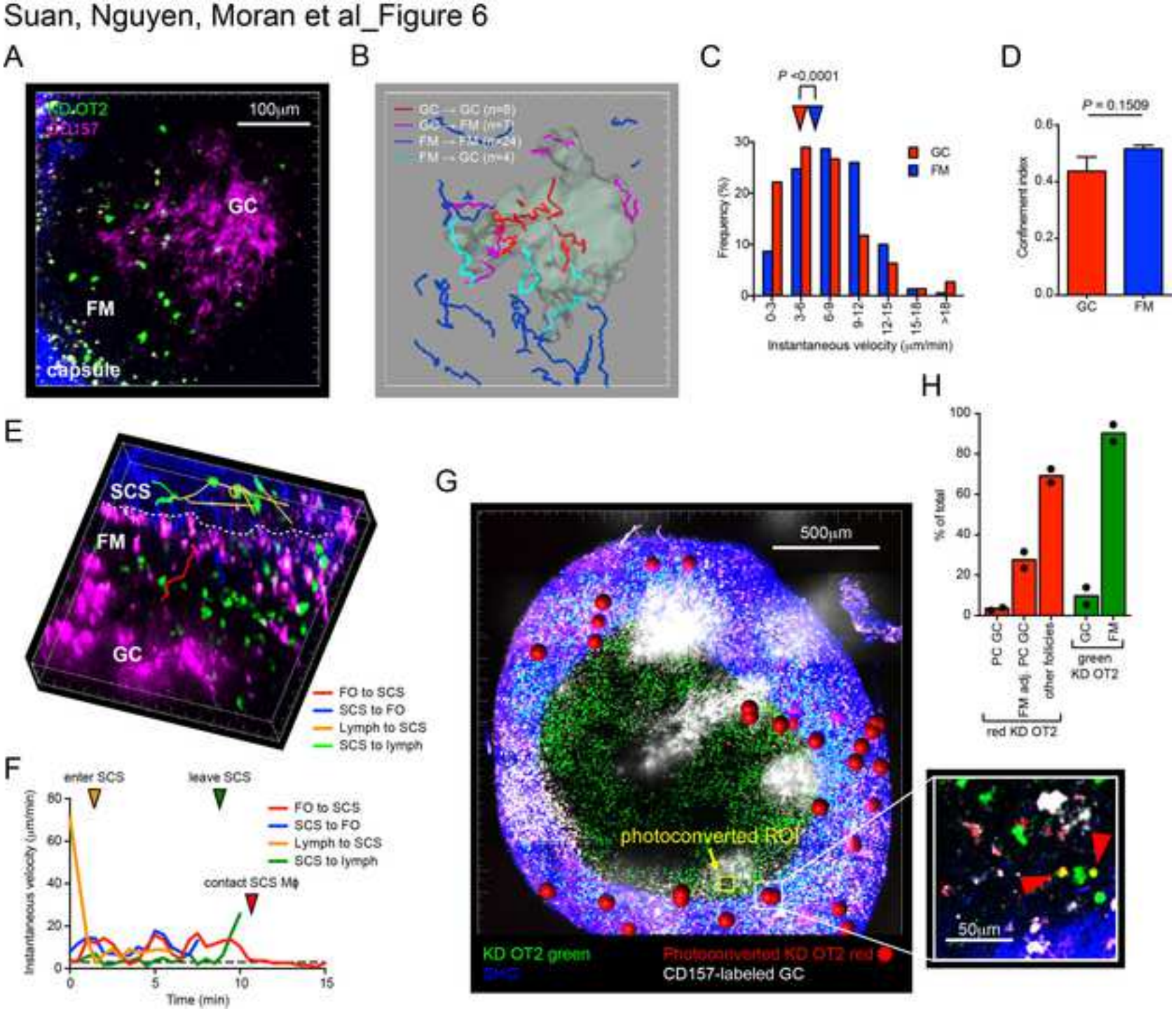

Figure 7
Click here to download high resolution image

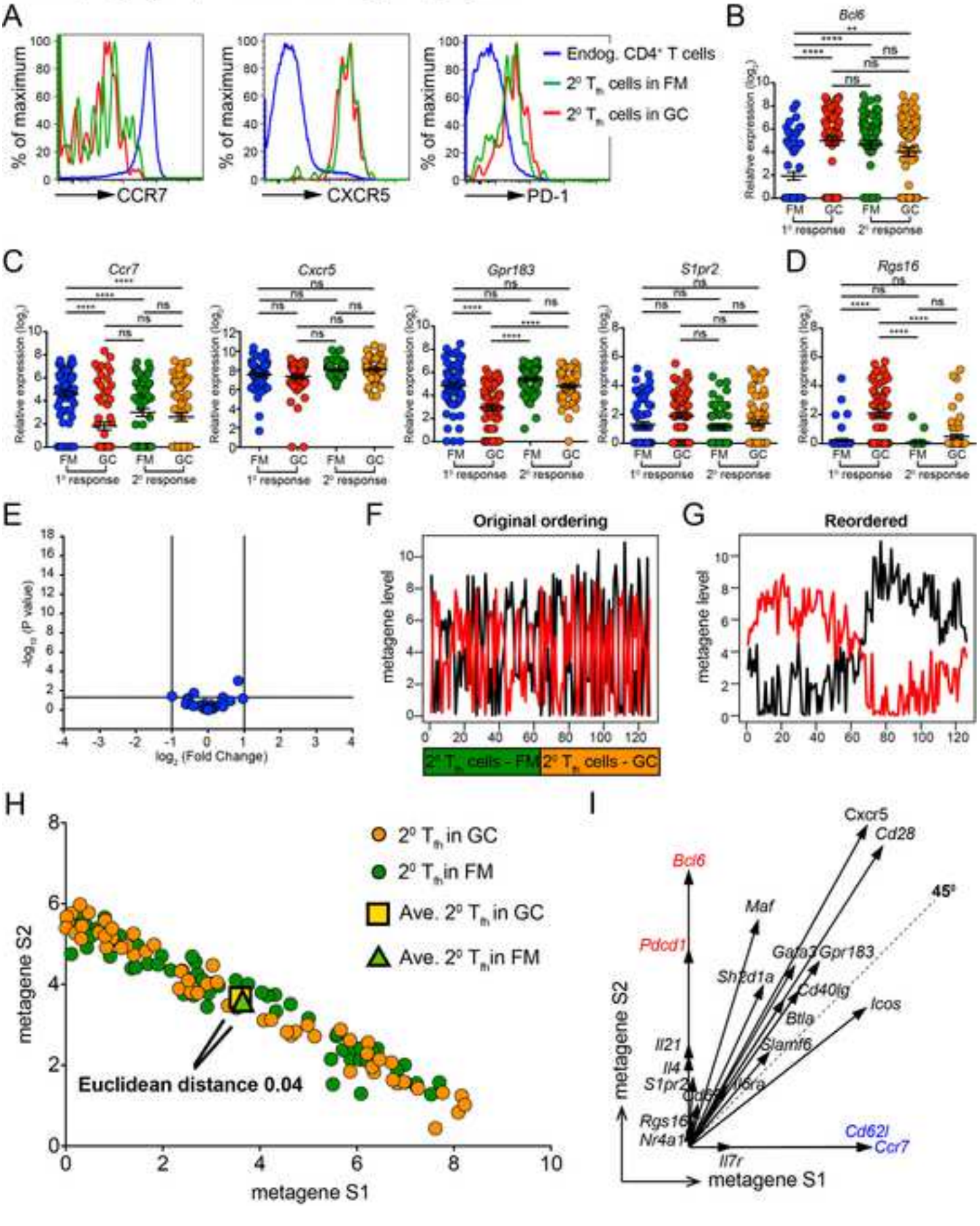

SUPPLEMENTAL EXPERIMENTAL PROCEDURES

Animals

Kaede transgenic mice (Tg(CAG-Kaede)#Kgwa) (Tomura et al., 2008) on the C57BL/6J background were crossed with OT2 TCR transgenic mice (004194; B6.Cg-Tg(TcraTcrb)425Cbn/J) (Barnden et al., 1998) to generate KD OT2 mice. SAP-deficient mice (025754; B6.129S6-*Sh2d1a*^{tm1Pls}/J) (Czar et al., 2001) on C57BL/6J background were used as recipients in adoptive transfer experiments. For retroviral transduction experiments, donor OT2 T cells were transduced and adoptively transferred into C57BL/6J mice either from the Australian Resources Centre or Australian BioResources. EBI2-deficient mice (Gpr183$^{tm1.2Rbr}$) (Gatto et al., 2009) were crossed with OT2 TCR transgenic mice to generate EBI2-deficient OT2 mice. CFP mice expressing cyan fluorescent protein under the β-actin promoter (004218; Tg(ACTB-ECFP)1Nagy/J) (Hadjantonakis et al., 2002) were used as a source of polyclonal B cells in some experiments as an additional fiducial label for the follicle. We generated transgenic mice expressing tdTomato by crossing floxed tdTomato reporter (007914; B6.Cg-*Gt(ROSA)26Sor*$^{tm14(CAG-tdTomato)Hze}$/J) (Madisen et al., 2010) with *ROSA26*-Cre mice that ubiquitously expresses Cre recombinase (003474; B6.129S4-*Gt(ROSA)26Sor*^{tm1Sor}/J) (Soriano, 1999). These were crossed with SW_{HEL} mice expressing a knock-in BCR against hen egg lysozyme (HEL) (Phan et al., 2003) to generate SW_{HEL} tdTomato mice. All mice were bred and maintained on a C57BL/6J background under specific-pathogen free conditions at the Australian BioResources and Garvan Institute Biological Testing Facility. Animal experiments were approved by the Garvan Institute of Medical Research/St Vincent's Hospital Animal Ethics Committee.

Immunisations, antigen trafficking and *in vivo* fiducial labeling

Donor KD OT2 T cells were enriched by negative depletion with biotinylated anti-B220 clone RA3-6B2, anti-CD11b clone M1/70, anti-CD11c clone HL3 and anti-Ly6C clone AL-21 (all from BD) and MACS anti-biotin magnetic beads (Miltenyi) as previously described (Phan et al., 2009). Purity of $CD4^+V_\alpha2^+$ KD OT2 was determined by FACS analysis was typically 70-80%. We

transferred 2.5×10^5 $CD4^+V_\alpha2^+$ KD OT2 into age and sex-matched 6-10 week old SAP-deficient recipient mice and allowed the cells to equilibrate before subcutaneous injection the next day with 20μg of OVA in Sigma Adjuvant System (SAS, Sigma) in the lower flank and base of the tail. Similar response kinetics were obtained with lower precursor frequencies (data not shown). Draining inguinal lymph nodes were then analysed by two-photon microscopy or FACS at indicated timepoints as described below. For memory responses, mice that had been immunised were rested for at least 28 days and then rechallenged with 40μg of OVA in SAS injected subcutaneously in the lower flank and base of the tail. SAP KO mice were used as recipients to remove competition from endogenous T cells. However, similar results were obtained in wildtype recipients (see **Fig. S1**). In some experiments, we also isolated antigen-specific B cells from SW_{HEL} tdTomato mice by MACS negative isolation using biotinylated anti-CD43 clone S7 (BD) and anti-CD11c clone HL3 (BD) and anti-biotin magnetic beads (Phan et al., 2007) and co-transferred 2.5×10^5 HEL^+ SW_{HEL} tdTomato B cells and $V_\alpha2^+$ $CD4^+$ KD OT2 into SAP-deficient recipients and immunised with 20μg HEL-OVA injected subcutaneously in the lower flank and tail base. HEL was conjugated to OVA peptide 329-337 (Mimotopes) as described (Gatto et al., 2009). To track antigen trafficking upon rechallenge, OVA or HEL (both from Sigma) was biotinylated and incubated in molar excess with SA-PE and unbound OVA-biotin or HEL-biotin was removed by size exclusion using an Amicon Ultra-4 centrifugal filter unit, MWCO 100kDa (Sigma). OVA-PE and HEL-PE was then injected subcutaneously to drain to the inguinal lymph node in mice immunised >28 days previously. Labeling of GCs is described below. To label SCS macrophages, we injected CD169 clone Ser-4 (UCSF Hybridoma Core) conjugated to either Alexa Fluor 555 or Alexa Fluor 680 (Invitrogen) (Phan et al., 2009). In some experiments, we also transferred CFP B cells as an additional fiducial label for the follicle.

In vivo fiducial labeling of GCs and validation of the labeling strategy

Previously we have injected anti-CD157 mAb clone BP-3 (UCSF Hybridome Core) subcutaneously in the flank and base of the tail the day before imaging to label the follicular stroma in a resting

lymph nodes (Phan et al., 2007). However, we have noticed that when CD157 is injected 3 or more days before imaging in immunised mice ("early injection of CD157"), it contracts to the centre of the follicle as shown by pulse-chase labeling with anti-CD157 conjugated to either Alexa Fluor 555 or Alexa Fluor 680 (Invitrogen) (see **Figure S3**). To visualize the microanatomical compartments labeled by the early injection of CD157, we set up immune responses to HEL-OVA with SW_{HEL} tDTomato B cells and KD OT2 T cells such that GCs are red due to the aggregation of SW_{HEL} GC B cells. As shown by the colocalization scatter plots (Dunn et al., 2011), 100% of CD157 signal colocalized with GC B cells with a Pearson's correlation coefficient of 0.71. Notably, 67% of GC B cells co-localized with the CD157 signal, indicating that it labeled a substructure within the GC. In contrast, there was no correlation between non-GC B cells and CD157 as only 4% of polyclonal CFP B cells were localized inside the CD157 labeled structure with a Pearson's correlation coefficient of 0.03. We next performed *ex vivo* wholemount staining of immunised lymph nodes with the classical GC marker PNA (Rose et al., 1980). This showed colocalization of of 100% of the CD157 within PNA^+ GCs with a Pearson's correlation coefficient of 0.25. Interestingly, only 36% of PNA^+ cells colocalized with CD157, again indicating that it was labeling a substructure within the GC. Finally, to identify the substructure labeled by early injection of CD157, we generated *in vivo* immune complexes using a previously described protocol (Phan et al., 2007) by passive transfer of 1 mg of polyclonal rabbit anti-BSA antibodies (Rocklands) the day before subcutaneous injection of 20μg of BSA conjugated to Alexa Fluor 680 (Invitrogen). This showed that 100% of the CD157 colocalized with the immune complexes and 43% of the immune complexes colocalized with CD157 with a Pearson's correlation coefficient of 0.61. Thus, early injection of CD157 labels a substructure in the GC which also traps immune complexes, most likely the FDC network in the light zone. We similarly confirmed this was true in secondary immune responses by colocalization of CD157 with PNA wholemount staining (100% colocalization of CD157 with PNA and 77% colocalization of PNA with CD157, Pearson's

correlation coefficient of 0.66). Thus, GCs defined by early injection of CD157 are the same between primary and secondary responses.

In addition to these two-photon microscopy validation studies, we also demonstrated conventional identification of GCs by histology (**Fig. S4**). For this, anti-CD157 mAb was injected subcutaneously on day 3 and lymph nodes from immunised mice were harvested on day 7 and snap frozen in OCT (TissueTek) and 10μm cryosections stained with anti-IgD mAb (clone 11-26, Southern Biotechnology) and anti-CD35 mAb (clone 8C12, BD Bioscience) as previously described (Phan et al., 2007). Analysis of serial sections showed that *in vivo* labeling with CD157 identified regions inside the follicle that only had a few IgD^+ naïve B cells. In contrast, the CD157 colocalized with CD35, which is expressed at high levels by follicular dendritic cells (FDCs) in the light zone of the GC (Allen and Cyster, 2008). Finally, in agreement with the wholemount staining and two-photon microscopy (**Fig. S3**), CD157 also labeled IgD^{lo} PNA^+ regions that are generally accepted histological criteria for GCs. Thus, early injection of CD157 identifies the FDC network inside GCs.

Retroviral transduction of primary T cells

Splenocytes were isolated from C57BL/6J mice and irradiated with 2000 rads using an X-RAD 320 (Precision X-Ray). Irradiated cells were then pulsed with 10μM OVA peptide 329-337 for 2 hours at 37˚C. 2×10^6 cells were then plated per well in a 24-well tissue culture plate and 1×10^6 $CD4^+$ T cells isolated by MACS purification from OT2 transgenic mice and 100U/ml recombinant murine IL-2 (Sigma) added per well. After 2 days of *in vitro* stimulation, OT2 T cells were retrovirally transduced with gene encoding EBI2 or empty cassette inserted into the MSCV2.2 retroviral vector carrying eGFP as an expression marker downstream of an IRES as previously described (Gatto et al., 2009). The next day, retrovirally transduced cells (10-30%) were FACS sorted for expression of eGFP, CD4 and $V_\alpha2$ TCR on a FACS Aria II (BD). We adoptively transferred 2.5×10^5 retrovirally transduced cells (>97% purity) into C57BL/6J recipient mice and immunised them 6 hours later

with 20μg OVA as described above. Draining inguinal lymph nodes were harvested 7 days later and scanned by two-photon microscopy to determine the localisation of transduced cells.

Two-photon microscopy and two-photon photoconversion

Intravital two-photon microscopy and TPP was performed as previously described with some minor changes (Chtanova et al., 2014). Briefly, mice were induced with 100mg/kg ketamine/5mg/kg xylazine and maintained on 1-2% isoflurane supplemented with 100% oxygen for anesthesia. Mice were kept warm on a custom heated SmartStage (Biotherm) set to 38˚C. The inguinal lymph node was mobilised along with the intact inguinal ligament in a skin flap and fixed on a base of thermal conductive T-putty (Thermagon Inc.) with VetBond tissue glue (3M). The cortical surface of the lymph node was exposed by microdisseting the skin and overlying fat and fascia layers. A rubber O-ring was used to stabilise the meniscus and in some experiments we also used Immersol (Carl Zeiss). Imaging was performed on a Zeiss 7MP two-photon microscope (Carl Zeiss) powered by a Chameleon Vision II ultrafast Ti-Sa laser (Coherent Scientific). Images were acquired with a W Plan-Apochromat 20×/1.0 DIC (UV)Vis-IR water immersion objective. Excitation wavelengths used were 810nm (to optimally detect photoconverted KD red), 870nm (to detect Alexa Fluor 555, Alexa Fluor 680, KD green) and 920nm (to detect KD green). Fluorescent images were acquired with a LBF 760 and BSMP 760 to enable detection of far-red signals. Non-descanned detectors were SP 485 (blue; SHG, Pacific Blue and CFP), BP 500-550 (green; KD), BP 565-610 (red; KD red, PE and Alexa Fluor 555) and BP 640-710 (far-red; Alexa Fluor 680). We also scanned explants to pinpoint the location of T_{fh} cells in some experiments. Wholemounts of the lymph node were stained with anti-B220 PE clone RA3-6B2 (BD), PNA-biotin (Vector Laboratories) and streptavidin-Pacific Blue (Biolegend) and imaged to show co-localisation of *in vivo* CD157-Alexa Fluor 680 label with PNA in the GC. TPP was achieved by real-time interactive scanning of ROIs with 840nm NIR excitation laser pulses for 2,000-5,000 cycles at varying laser power intensities to achieve optimal photoconversion as determined by loss of green and acquisition of red signal

(Chtanova et al., 2014). TPP was non-toxic as demonstrated by the fact that cells within the photoconversion volume continued to migrate with the same velocities before, during and after TPP.

Image analysis and cell tracking

Raw image files were imported into Imaris (Bitplane) and image intensities and thresholds adjusted and a Guassian filter used to reduce noise. Drift correction was applied and cells were detected using the spot detection function and the automatically generated tracks were manually verified. Cells were identified using the Spot detection function to enable counting of red and green cells in the GC and FM. Motility parameters were extracted from the Imaris Statistics function and calculated as described (Matheu et al., 2011). Note the "confinement index" (calculated as "track straightness" in Imaris) is defined as the displacement divided by the total track length and does not directly measure the confinement of cells to a particular compartment *per se* but rather the likelihood a cell will move in a straight line and thereby leave a compartment. In some experiments, surfaces were applied to delineate the boundaries of GCs using the Imaris Surface function and individual tracks assigned in relation to these boundaries. For these analyses, the GC was defined as the CD157-rich centre of the follicle and the FM was defined as the surrounding CD157-negative area between the GC and capsule. For analysis of cell behaviour when distant (>20μm) and proximal (<20μm) to SCS macrophages, individual tracks were manually checked at each timepoint to determine their position in relation to the $CD169^+$ SCS macrophages. Time-lapse images were exported, compiled and annotated in Adobe AfterEffects (Adobe), and movies converted using HandBrake (https://handbrake.fr).

FACS analysis and single cell FACS sorting

Draining inguinal lymph nodes were harvested and single cell suspensions prepared for FACS analysis as described (Phan et al., 2009). Antibodies used were anti-IgD Alexa Fluor 647 clone 11-26c.2a (Biolegend), anti-Fas PE clone Jo2 (BD), anti-$V_\alpha 2$ Pacific Blue or APC clone B20.1 (eBioscience), anti-B220 Pacific Orange clone RA3-B62 (BD), anti-CD4 Pacfic Blue or Brilliant Violet 785 clone RM4-5 (BioLegend), purified anti-CXCR5 clone 2G8 (BD) detected with

biotinylated affinity purified donkey anti-rat IgG (H+L) Fab_2 (Jackson ImmunoResearch Laboratories) and SA-PE-Cy7 (eBioscience), anti-CCR7 APC or Brilliant Violet 421 clone 4B12 (eBioscience) and anti-PD-1 PE or APC clone J43 (BD). Staining for CXCR5 was followed by blocking with normal rat serum (Jackson ImmunoResearch Laboratories), and staining for CCR7 was performed at 37˚C. Staining for EBI2 was performed with affinity purified polyclonal chicken anti-EBI2 antibodies (Gatto et al., 2013) conjugated to Alexa Fluor 647. Data was acquired on an LSR II SORP (BD). Single cell FACS sorting was performed into a 96-well skirted PCR plate on a FACS Aria II as previously described (Phan et al., 2005).

Single cell RT-qPCR

RNA was isolated from single FACS sorted cells using the Ambion Single Cell to CT kit (Life Technologies) according to the manufacturer's instructions. Briefly, single $DAPI^{neg}$ photoconverted red cells were sorted into 10µl of single cell lysis/Dnase I solution in a 96-well plate kept chilled at 4˚C in the collection chamber of a FACS Aria II. Batches of 32 single cells were sorted and brought to room temperature for 5 minutes before 1µl of stop solution was added for 2 minutes. 4.5µl of RT mix was then added and incubated for 10 minutes at 25˚C, 60 minutes at 42˚C and 5 minutes at 85˚C. We then added 11µl of the PreAmp Mix/Taqman assay and preamplified the transcripts by holding at 95˚C for 10 minutes then running 14 cycles of 95˚C for 15 followed by 60˚C for 4 minutes in a C1000 Thermocycler (BioRad). We then performed RT-qPCR on the diluted preamplified product using the 7900HT Fast Real-Time PCR System (Applied Biosystems).

Pre-processing of single cell gene expression data

Raw cycle threshold (Ct) values were subtracted from a cutoff value of 35 to obtain dCt values. These were then expressed as Relative Quantitation (RQ) values ($2^{\Delta CT}$). The data was $\log_2$ transformed using the LogTransform module in GenePattern (https://pwbc.garvan.org.au/gp), which sets any negative values (arising from samples with gene expression below the threshold Ct 35) to zero. Single cell expression datasets were quantile normalized using the NormalizeColumns module in GenePattern (**Figure S5**). For the purpose of normalization, zero values were removed from the

dataset and replaced afterwards.

Gene expression analysis by NMF

Gene expression analyses were carried out on a complete log-transformed normalized dataset of 32 genes across 252 single-cell samples (8064 transcripts). Seven genes (*Foxp3, Ifng, Il2ra, Prdm1, Rorc, Slamf8* and *Tbx1*) were not expressed at all and excluded from analysis to leave a 25 gene dataset. LimmaGP, a GenePattern implementation of the Limma (Smyth, 2004) BioConductor library module in GenePattern, was used to identify differentially expressed genes between user-defined cell populations (based on micro-anatomical location), with a false discovery rate (FDR) of <0.05. To identify cell populations without *a priori* classification, NMF was coupled with a model selection method, NMFConsensus (Brunet et al., 2004) as implemented in GenePattern, which determines the most robust and reproducible number of subclasses that exist within the dataset. Heatmaps were generated using the HeatMapViewer module in GenePattern and metagenes and vectors plotted in R (http://www.R-project.org).

Statistical analysis

Data was analysed with Prism software (GraphPad). For comparison between two normally distributed groups we used a two-tailed unpaired Student's *t*-test with Welch's correction, and for more than two groups we used one-way ANOVA with Tukey's correction for multiple comparisons. Non-parametric data was analysed by Mann-Whitney *U* test. Differences between multiple paired measurements were analysed by the Wilcoxon signed-rank test. Colocalization was analysed by calculating the Pearson's correlation coefficient in Imaris.

References

Allen, C.D., and Cyster, J.G. (2008). Follicular dendritic cell networks of primary follicles and germinal centers: phenotype and function. Seminars in immunology *20*, 14-25.

Barnden, M.J., Allison, J., Heath, W.R., and Carbone, F.R. (1998). Defective TCR expression in transgenic mice constructed using cDNA-based alpha- and beta-chain genes under the control of heterologous regulatory elements. Immunology and cell biology *76*, 34-40.

Brunet, J.P., Tamayo, P., Golub, T.R., and Mesirov, J.P. (2004). Metagenes and molecular pattern discovery using matrix factorization. Proceedings of the National Academy of Sciences of the United States of America *101*, 4164-4169.

Chtanova, T., Hampton, H.R., Waterhouse, L.A., Wood, K., Tomura, M., Miwa, Y., Mackay, C.R., Brink, R., and Phan, T.G. (2014). Real-time interactive two-photon photoconversion of recirculating lymphocytes for discontinuous cell tracking in live adult mice. Journal of biophotonics *7*, 425-433.

Czar, M.J., Kersh, E.N., Mijares, L.A., Lanier, G., Lewis, J., Yap, G., Chen, A., Sher, A., Duckett, C.S., Ahmed, R., and Schwartzberg, P.L. (2001). Altered lymphocyte responses and cytokine production in mice deficient in the X-linked lymphoproliferative disease gene SH2D1A/DSHP/SAP. Proceedings of the National Academy of Sciences of the United States of America *98*, 7449-7454.

Dunn, K.W., Kamocka, M.M., and McDonald, J.H. (2011). A practical guide to evaluating colocalization in biological microscopy. American journal of physiology. Cell physiology *300*, C723-742.

Gatto, D., Paus, D., Basten, A., Mackay, C.R., and Brink, R. (2009). Guidance of B cells by the orphan G protein-coupled receptor EBI2 shapes humoral immune responses. Immunity *31*, 259-269.

Gatto, D., Wood, K., Caminschi, I., Murphy-Durland, D., Schofield, P., Christ, D., Karupiah, G., and Brink, R. (2013). The chemotactic receptor EBI2 regulates the homeostasis, localization and immunological function of splenic dendritic cells. Nature immunology *14*, 446-453.

Hadjantonakis, A.K., Macmaster, S., and Nagy, A. (2002). Embryonic stem cells and mice expressing different GFP variants for multiple non-invasive reporter usage within a single animal. BMC biotechnology *2*, 11.

Madisen, L., Zwingman, T.A., Sunkin, S.M., Oh, S.W., Zariwala, H.A., Gu, H., Ng, L.L., Palmiter, R.D., Hawrylycz, M.J., Jones, A.R., *et al.* (2010). A robust and high-throughput Cre reporting and characterization system for the whole mouse brain. Nature neuroscience *13*, 133-140.

Matheu, M.P., Cahalan, M.D., and Parker, I. (2011). Immunoimaging: studying immune system dynamics using two-photon microscopy. Cold Spring Harbor protocols *2011*, pdb top99.

Phan, T.G., Amesbury, M., Gardam, S., Crosbie, J., Hasbold, J., Hodgkin, P.D., Basten, A., and Brink, R. (2003). B cell receptor-independent stimuli trigger immunoglobulin (Ig) class switch recombination and production of IgG autoantibodies by anergic self-reactive B cells. J Exp Med *197*, 845-860.

Phan, T.G., Gardam, S., Basten, A., and Brink, R. (2005). Altered migration, recruitment, and somatic hypermutation in the early response of marginal zone B cells to T cell-dependent antigen. J Immunol *174*, 4567-4578.

Phan, T.G., Green, J.A., Gray, E.E., Xu, Y., and Cyster, J.G. (2009). Immune complex relay by subcapsular sinus macrophages and noncognate B cells drives antibody affinity maturation. Nat Immunol *10*, 786-793.

Phan, T.G., Grigorova, I., Okada, T., and Cyster, J.G. (2007). Subcapsular encounter and complement-dependent transport of immune complexes by lymph node B cells. Nat Immunol *8*, 992-1000.

Rose, M.L., Birbeck, M.S., Wallis, V.J., Forrester, J.A., and Davies, A.J. (1980). Peanut lectin binding properties of germinal centres of mouse lymphoid tissue. Nature *284*, 364-366.

Smyth, G.K. (2004). Linear models and empirical bayes methods for assessing differential expression in microarray experiments. Statistical applications in genetics and molecular biology *3*, Article3.

Soriano, P. (1999). Generalized lacZ expression with the ROSA26 Cre reporter strain. Nature genetics *21*, 70-71.

Tomura, M., Yoshida, N., Tanaka, J., Karasawa, S., Miwa, Y., Miyawaki, A., and Kanagawa, O. (2008). Monitoring cellular movement in vivo with photoconvertible fluorescence protein "Kaede" transgenic mice. Proceedings of the National Academy of Sciences of the United States of America *105*, 10871-10876.

Supplemental Table 1. Alphabetical list of 32 genes assayed by multiplex single cell RT-qPCR. Genes highlighted in red were non-T_{fh} cell genes that were not expressed at all, or only expressed at low levels in 1 or 2 out of 254 cells isolated and therefore excluded from NMF analysis.

B2m
Bcl6
Btla
Ccr7
Cd28
Cd40lg
Cd62l
Cd69
Cxcr5
Foxp3
Gapdh
Gata3
Gpr183
Icos
Il21
Il2ra
Il4
Il6ra
Il7r
Infg
Maf
Nr4a1
Pdcd1
Prdm1
Rgs16
Rn18s
Rorc
S1pr2
Sh2d1a
Slamf6
Slamf8
Tbx1

SUPPLEMENTAL FIGURE LEGENDS

Figure S1. Kinetics of the primary T_{fh} cell response. (**A**) Experimental system for generating T_{fh} cells in the lymph node. 2.5×10^5 $V_\alpha2^+CD4^+$ KD OT2 cells are adoptively transferred into SAP-deficient recipients. The next day mice are immunised subcutaneously with 20μg OVA in Sigma Adjuvant System (SAS) in the lower flank and base of the tail the next day. At indicated timepoints mice were sacrificed and lymph nodes analysed by FACS. (**B**) Representative FACS plots of mice from indicated timepoints showing CCR7, CXCR5 and PD-1 expression gated on green $CD4^+$ KD OT2 cells. (**C**) Total cell counts of green $CD4^+$ KD OT2 cells, $CXCR5^+PD\text{-}1^+$ KD OT2 and IgD^+Fas^{hi} GC B cells. The T_{fh} response peaks on day 5, two days before the peak of the GC response. (**D**) Immune response in wildtype recipient mice. 2.5×10^5 $V_\alpha2^+CD4^+$ KD OT2 cells are adoptively transferred into wildtype recipients. Mice were immunised as in (**A**) and total cell counts of green $CD4^+$ KD OT2 cells, $CXCR5^+PD\text{-}1^+$ KD OT2 and IgD^+Fas^{hi} GC B cells enumerated. (**E**) 3D reconstruction of follicle imaged by two-photon microscopy on day 9 showing confinement of primary GC (red tracks) and FM T_{fh} cells (green tracks) in wildtype recipient mice. KD OT2 cells are green. SW_{HEL} B cells (red) predominantly localise in the GC and polyclonal B cells (cyan) outside in the FM.

Figure S2. T_{fh} cells colonised the follicle on day 5 before GCs have formed. (**A**) Mosaic tiled image of lymph node from day 5 immunised mice. B220 (red), KD (green) and CD4 (blue). (**B**) Experimental system for optical marking of KD OT2 cells in the follicle. Mice are immunised as shown in **Figure S1** and on day 6 the B cell follicle labeled by adoptive transfer of $1\text{-}3\times10^7$ CFP B cells and subcutaneous injection of anti-CD157 Alexa Fluor 680. On day 5 the lymph node was harvested and cells in the follicle optically marked by TPP. (**C**) Maximal intensity projection (332×332×99μm volume) of lymph node follicle immediately after TPP. Dashed box indicate the targeted ROI. Follicular stroma labeled with anti-CD157 mAb (magenta), polyclonal CFP B cells (cyan), unphotoconverted KD OT2 cells (green), photoconverted KD OT2 (red). (**D**) FACS analysis

of photoconverted lymph node showing cells in the follicle have a $CXCR5^{+}PD\text{-}1^{+}$ T_{fh} cell phenotype. (**E**) FACS analysis of sham photoconverted lymph node showing specificity of the optical marking.

Figure S3. Fiducial labeling of the primary and secondary GC with anti-CD157 mAb injected >3 days before imaging. (**A**) Pulse-chase labeling with anti-CD157 mAb shows that injection 3 days before imaging (red) results in contraction of the signal to the centre of the follicle compared to injection one day before imaging (green) which results in labeling of the entire follicle. Collagen in the capsule from SHG is blue. (**B**) Contraction of the anti-CD157 mAb signal co-localises with GC B cells. 2.5×10^{5} HEL-binding SW_{HEL} tdTomato B cells (red) and $V_{\alpha}2^{+}CD4^{+}$ KD OT2 cells (green) are adoptively co-transferred into SAP-deficient recipients. Mice are then subcutaneously with 20μg HEL-OVA in SAS in the lower flank and base of the tail the next day. On day 4 anti-CD157 mAb (magenta) was injected subcutaneously to drain to the same lymph node and polyclonal CFP B cells (cyan) were injected on day 6. Mice were sacrificed on day 7 and analysed by two-photon microscopy. Colocalization scatter plot shows 100% of the CD157 signal colocalized with SW_{HEL} GC B cells and 67% of GC B cells colocalized with CD157, with a Pearson's correlation coefficient of 0.71. In contrast, the majority of naïve polyclonal B cells are in the FM outside the GC and colocalization analysis showed no correlation as only 4% of polyclonal CFP B cells colocalized with CD157 and Pearson's correlation coefficient was only 0.03. Also note some SW_{HEL} B cells are located in the FM and the anti-CD157 mAb labels a region smaller than the GC B cells. (**C**) Contraction of anti-CD157 mAb (red) co-localises with GC marker PNA. Lymph nodes were harvested on day 7 and wholemounts fixed and stained with PNA-biotin and detected with SA-Pacific Blue (blue). KD OT2 cells are green. The anti-CD157 mAb contracts to the centre of the GC suggesting it labels a structure distinct from the GC B cells. Also note some of the anti-CD157 mAb trapped in the interfollicular region. Colocalization scatter plot shows 100% of the CD157 signal colocalized with PNA and 36% of PNA colocalized with CD157 with a Pearson's correlation coefficient of 0.25. Note Pacific Blue, the blue component of CFP and SHG were all

detected in the same channel and therefore the colocalization of blue with red channel is underestimated. Thus, contraction of CD157 signals labels a network structure in the GC and not GC cells *per se*. Also note autofluorescence from SCS and tingible body macrophages. (**D**) Contraction of anti-CD157 mAb co-localises with the FDC network. KD OT2 cells (green) were adoptively transferred and mice immunised as above. On day 4, anti-CD157 mAb (magenta) was injected subcutaenously. On day 6, BSA-anti-BSA immune complexes (magenta) were generated *in vivo* to drain to the immunised lymph nodes and polyclonal CFP B cells (cyan) adoptively transferred. Lymph nodes were imaged on day 7 by two-photon microscopy. Colocalization scatter plot shows 99% of the CD157 signal colocalized with *in vivo* generated immune complexes and 43% of immune complexes colocalized with CD157 with a Pearson's correlation coefficient of 0.61. Thus, early injection of anti-CD157 labels the FDC network. Collagen in the capsule is blue from SHG. (**E**) Secondary GC labeling with early anti-CD157 injection. 2.5×10^5 $V_\alpha2^+CD4^+$ KD OT2 cells (green) were adoptively co-transferred into SAP-deficient recipients and immunized with OVA as above. 28 days later mice were rechallenged subcutaneously with OVA in SAS. Anti-CD157 mAb was injected on day 1 and the draining lymph node imaged on day 5 post secondary challenge. Colocalization scatter plot shows 100% of the CD157 signal colocalized PNA and 77% of PNA colocalized with CD157 with a Pearson's correlation coefficient of 0.66. Note there are no CFP B cells in this experiment and there is better colocalization of the blue and far-red channel compared to (**C**). **Further validation of the *in vivo* GC labeling strategy by conventional histology.** (**F**) Mice were immunized and GCs were labeled *in vivo* by subcutaneous injection of CD157 (pseudocoloured green) on day 3. Lymph nodes were harvested on day 7 and cryosections stained for IgD to identify naïve B cells (red). CD157 labels a region in the centre of the follicle which is low for IgD. (**G**) Serial cryosection of same GC from (**F**) was stained for CD35 (red) to reveal colocalization of CD157 (pseudocoloured green) with the FDC network which expresses high levels of CD35. (**H**) Double-staining of cryosections from (**F**) with IgD (red) and PNA (blue)

showed that *in vivo* injection of CD157 on day 3 labels a region in the centre of the follicle that is IgD low and PNA negative that is classically defined as the GC.

Figure S4. Unbiased NMF analysis of primary T_{fh} cell gene expression signatures. (**A**) Consensus matrices and cophenetic coefficients for NMF model selection at rank *k* = 2-5. (**B**) Heatmap showing normalised relative expression values for the 25 genes across 62 FM and 64 GC primary T_{fh} cells. NMF reduced the 25 gene × 126 cell matrix into a rank-2 model. (**C**) Heatmaps of the factorised data before and (**D**) after re-ordering of the genes and samples into metagenes and clusters, respectively.

Figure S5. Kinetics of the secondary T_{fh} cell response. (**A**) Experimental system for generating secondary T_{fh} cell responses. KD OT2 cells are adoptively transferred into SAP-deficient recipient mice as described in **Figure S1** and mice rested for 28-104 days before rechallenge with 40μg OVA. At indicated timepoints mice were sacrificed and lymph nodes analysed by FACS. (**B**) Representative FACS plots of mice from indicated timepoints showing CCR7, CXCR5 and PD-1 expression gated on green $CD4^+$ KD OT2 cells. (**C**) Total cell counts of $CD4^+$ KD OT2 cells, $CXCR5^+PD\text{-}1^+$ KD OT2 and IgD^+Fas^{hi} GC B cells. Note the T_{fh} response peaks on day 3, two days before the peak of the GC response. This is two days earlier than the primary T_{fh} response. Also note secondary T_{fh} cells express high levels of CXCR5 and PD-1 from the beginning of the response, in contrast to primary T_{fh} cells which require maturation before they express high levels of these surface molecules.

Figure S6. Unbiased NMF analysis of secondary T_{fh} cell gene expression levels. (**A**) Consensus matrices and cophenetic coefficients for NMF model selection at rank *k* = 2-5. (**B**) Heatmap showing normalised relative expression values for the 25 genes across 63 FM and 63 GC secondary T_{fh} cells. NMF reduced the 25 gene × 126 cell matrix into a rank-2 model. (**C**) Heatmaps of the

factorised data before and (**D**) after re-ordering of the genes and samples into metagenes and clusters, respectively.

Fig. S7. Unbiased cluster analysis of all four cell populations from the primary and secondary response. KD OT2 T_{fh} cells localized in the FM and GC from primary (**Fig. S5**) and secondary responses (**Fig. S6**) were photoconverted and single cells sorted for multiplex RT-qPCR as described. (**A**) Consensus matrices and cophenetic coefficients for NMF model selection at rank *k* = 2-5. (**B**) Expression of the identified metagenes f0 (k2) and f1 (k2) by single cells belonging to the four cell populations based on rank *k* = 2 cluster model. Red circle = primary GC, blue circle = primary FM, orange circle = secondary GC, green circle = secondary FM. (**C**) Metagene expression by the centroid of the four cell populations. The Euclidean distance between the centroids are shown. In this model, cells clustered into two groups with metagene f0 (k2) expressed predominantly by single cells from primary GC group and metagene f1 (k2) by single cells from primary FM, secondary GC and secondary FM groups. Red triangle = primary GC, blue triangle = primary FM, orange triangle = secondary GC, green triangle = secondary FM. (**D**) Expression of the identified metagenes f0 (k3), f1 (k3) and f2 (k3) by single cells belonging to the four cell populations based on rank *k* = 3 cluster model. Red circle = primary GC, blue circle = primary FM, orange circle = secondary GC, green circle = secondary FM. (**E**) Metagene expression by the centroid of the four cell populations. The Euclidean distance between the centroids are shown. In this model, cells clustered into three groups with metagene f0 (k3) expressed predominantly by single cells from primary GC group, metagene f1 (k3) by single cells from both secondary GC and secondary FM groups, and metagene f2 (k3) by single cells from primary FM group. Red circle = primary GC, blue circle = primary FM, orange circle = secondary GC, green circle = secondary FM.

SUPPLEMENTAL MOVIE LEGENDS

Movie S1. Primary T_{fh} cells are confined to the GC. Time-lapse images and animation (398×390×75μm volume) showing the migration pattern of T_{fh} cells on day 7 of the primary response. KD OT2 cells, green; CD157, magenta; SHG from collagen in the capsule, blue. Time stamp hh:mm:ss. The GC boundary was determined by applying a suface in Imaris and cell tracks assigned based on their location and direction. See also **Figures 1A and B.**

Movie S2. Primary T_{fh} cells are retained in the follicle of origin. Primary T_{fh} cells in the GC were photoconverted and mice allowed to recover from anesthesia before the lymph node was optically sectioned by two-photon microscopy 24 hours later. Photoconverted GC T_{fh} cells, red; unphotoconverted T_{fh} cells, green; CD157, magenta; polyclonal CFP B cells, cyan; SHG from collagen in the capsule, blue. See also **Figures 1E and F.**

Movies S3. Identification of memory T cells in proximity to SCS macrophages in the B cell follicle. First movie shows z-stacks from immune lymph node of mice on day 35. KD OT2 T cells are green, follicular stroma labeled by injection of CD157 the day before imaging magenta, polyclonal B cells cyan, capsule blue. See also **Figure 4A**. Second movie shows of z-stacks from immune lymph node of mice on day 30. KD OT2 T cells are green, $CD169^+$ macrophages magenta, capsule blue. See also **Figure 4B**.

Movie S4. Follicular memory T cells cells reside in the subcapsular region of the lymph node where they scan SCS macrophages. First movie shows rendered 212×212×99μm volume of draining lymph node 37 days after primary immunisation. Memory T_{fh} cells (green) localise in the periphery adjacent to SCS macrophages (CD169, magenta). Tracks of follicular memory T cells scanning SCS macrophages (red line) and migrating from the follicle up to the SCS macrophages (blue lines) are shown. Time stamp hh:mm:ss. See also **Figure 4C.** Second movie shows time-lapse images (106×106×51μm volume) 37 days after primary immunisation showing two follicular memory T cells (green) actively scanning SCS macrophages (CD169, magenta). Surface contact between the cells are shown as yellow COLOC channel generated by Imaris. This is distinct from

white signal from overlap of green and magenta in the *z*-axis. Note polyclonal CFP B cells (cyan) also scan SCS macrophages. Time stamp hh:mm:ss. See also **Figure 4H**.

Movie S5. Secondary T_{fh} cells are activated by SCS macrophages and proliferate in the subcapsular region. Mice were rested for 28 days and draining lymph node imaged 2 days after rechallenge with OVA. First movie compiled from time-lapse images show secondary T_{fh} cells (green) in contact with SCS macrophages (CD169, red) have a rounded celll morphology and have arrested compared to the motile cells in the follicle (CD157, magenta) which migrate with elongated shapes. Time stamp hh:mm:ss. See also **Figure 5D.** Second movie compiled from time lapse images of follicle in draining lymph node 2 days after secondary antigen challenge. KD OT2 are green. A rounded T_{fh} cell (yellow arrow) is shown undergoing cell division in contact with SCS macrophage (CD169, red). Note the elongated cells migrating in the follicle (CD157, magenta). Time stamp hh:mm:ss. See also **Figure 5G.**

Movie S6. Secondary T_{fh} cells leave the GC. Time-lapse images and animation showing (393×407×96μm volume) showing the migration pattern of T_{fh} cells 5 days after secondary antigen challenge in a mouse that was initially immunised 28 days earlier. KD OT2 cells, green; CD157, magenta; SHG from collagen in the capsule, blue. Time stamp hh:mm:ss. The GC boundary was determined by applying a suface in Imaris and cell tracks assigned based on their location and direction. See also **Figures 6A and B.**

Movie S7. Secondary T_{fh} cells enter and leave the follicle via the lymphatic flow in the SCS. First movie compiled from time-lapse images of 425×425×87μm volume 5 days after secondary challenge in mouse that was initially immunised 35 days earlier. Labels identify the SCS, subcapsular sinus; FM, follicular mantle; GC, germinal centre (contracted CD157, magenta). KD OT2 cells, green; unphotoconverted T_{fh} cells, green; CD157, magenta; SHG from collagen in the capsule, blue. Annotation shows secondary T_{fh} cells crawling through the floor of the SCS to enter the lumen (yellow triangle), detaching and leaving the follicle (red circle), flowing past in the lymphatic stream (red triangle) and arriving in the follicle (white triangle). Note even at this late

timepoint a T_{fh} cell can be seen dividing on the process of a SCS macrophage (arrow). See also **Figure 6E and F.** Second movie shows z-stacks from lymph node in which secondary T_{fh} cells in the GC were photoconverted and mice allowed to recover from anesthesia before the lymph node was optically sectioned by two-photon microscopy 24 hours later. 3D mosaic tile of one lobe of the inguinal lymph node used to identify photoconverted red cells in Imaris is shown. Photoconverted GC T_{fh} cells, red; unphotoconverted T_{fh} cells, green; CD157, magenta; SHG from collagen in the capsule, blue. See also **Figure 6G and H**.

Supplemental Text & Figures

Click here to download high resolution image

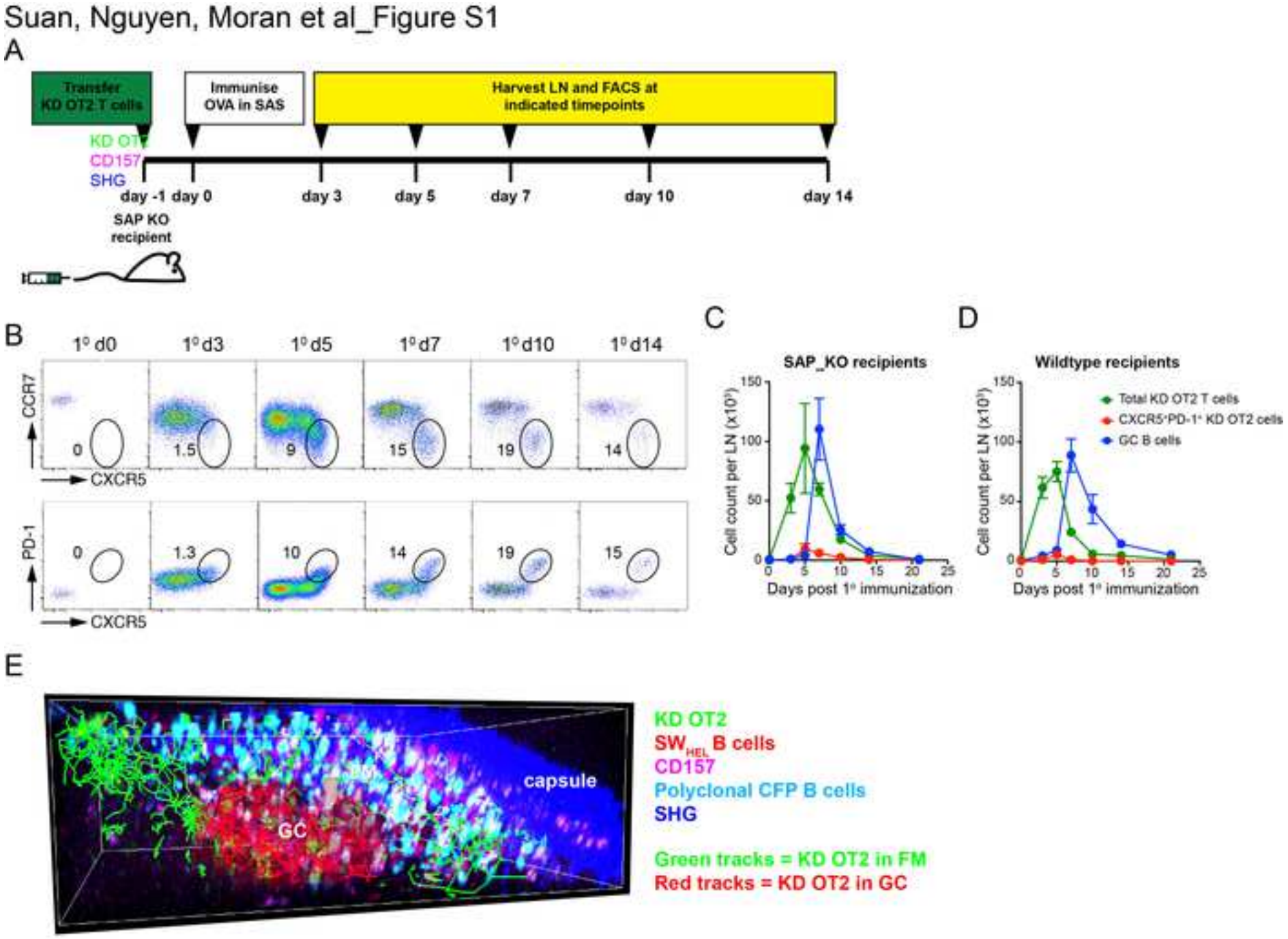

Supplemental Text & Figures

Click here to download high resolution image

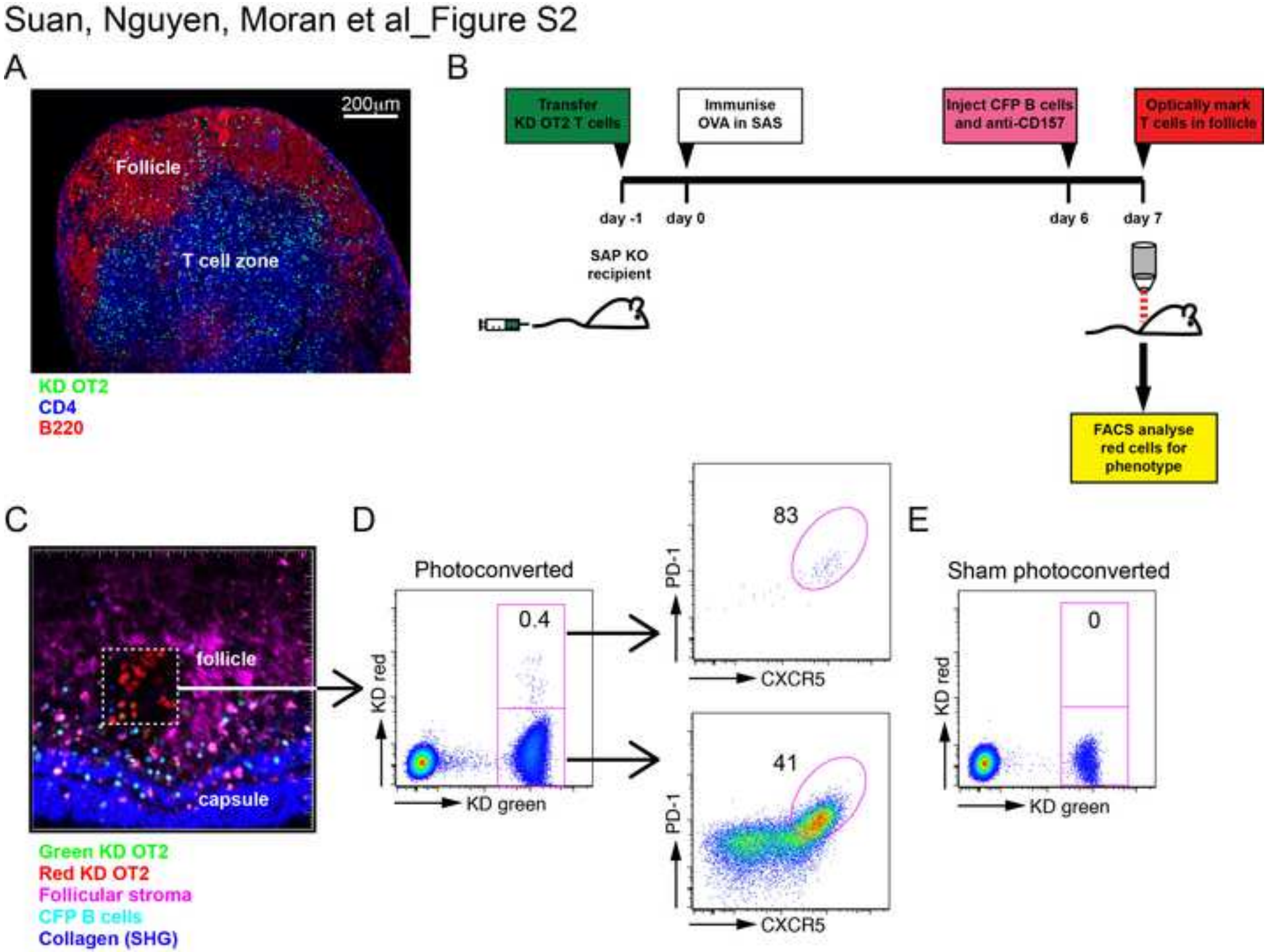

Supplemental Text & Figures

Click here to download high resolution image

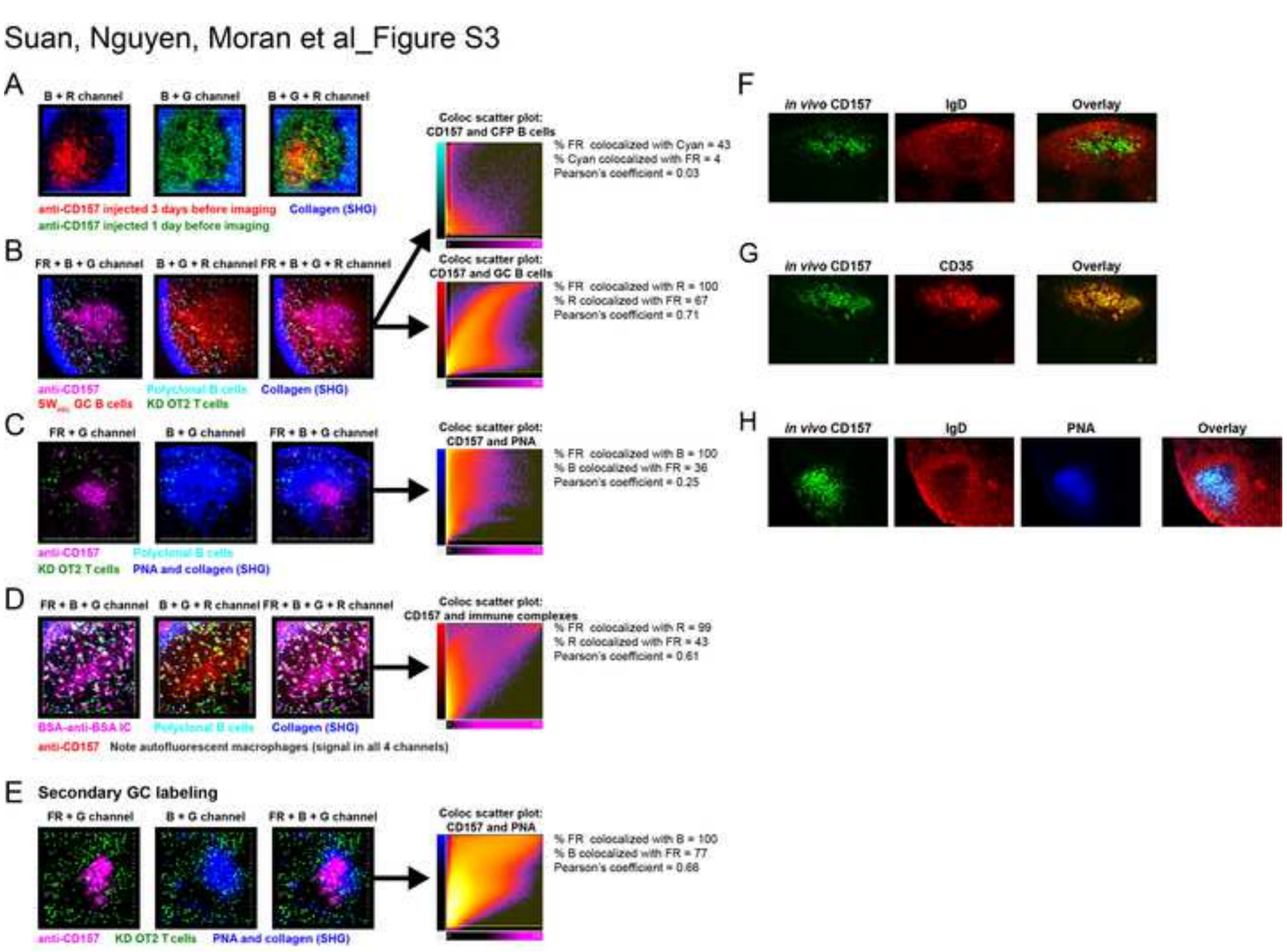

Supplemental Text & Figures

Click here to download high resolution image

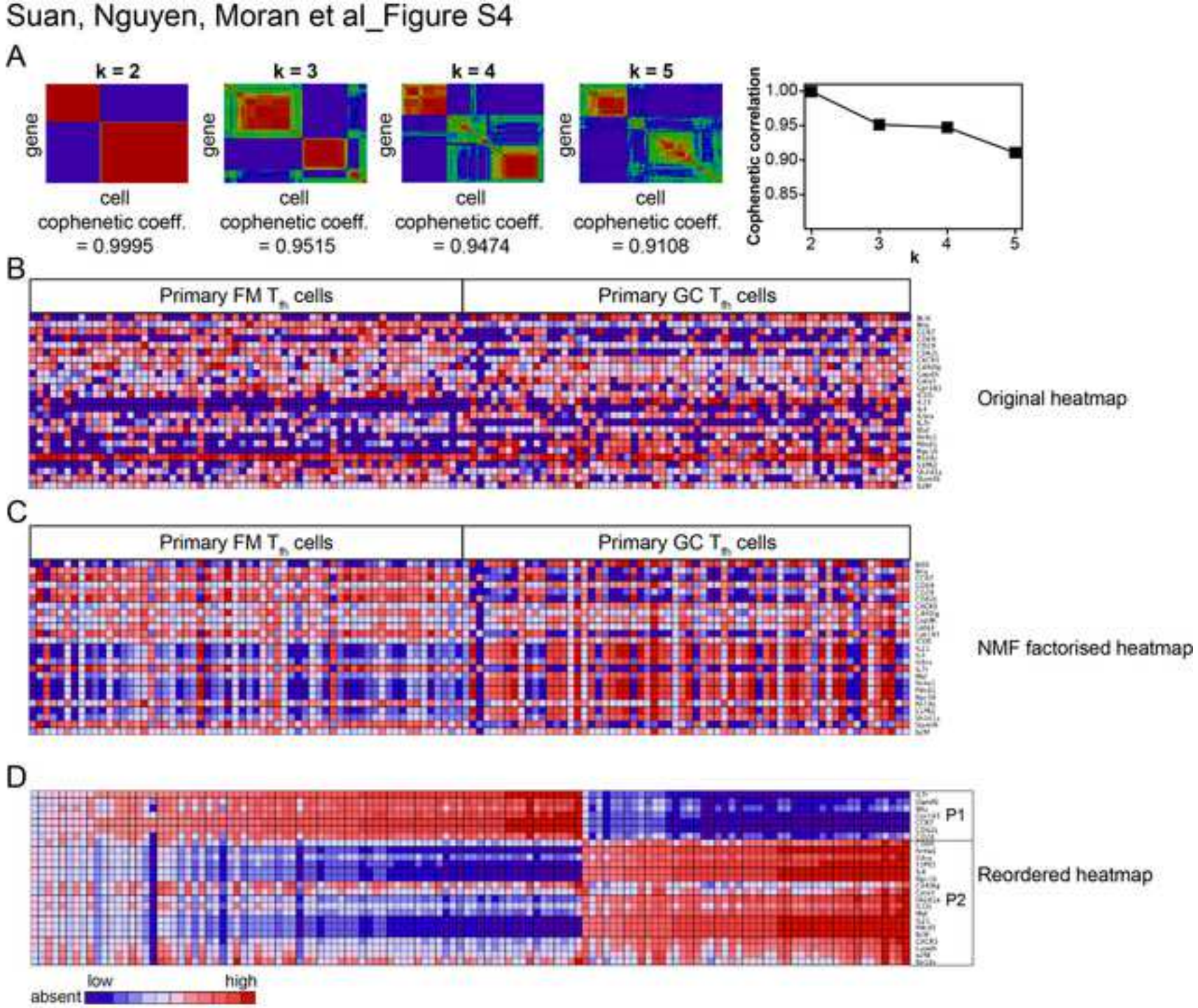

Supplemental Text & Figures

Click here to download high resolution image

Suan, Nguyen, Moran et al_Figure S5

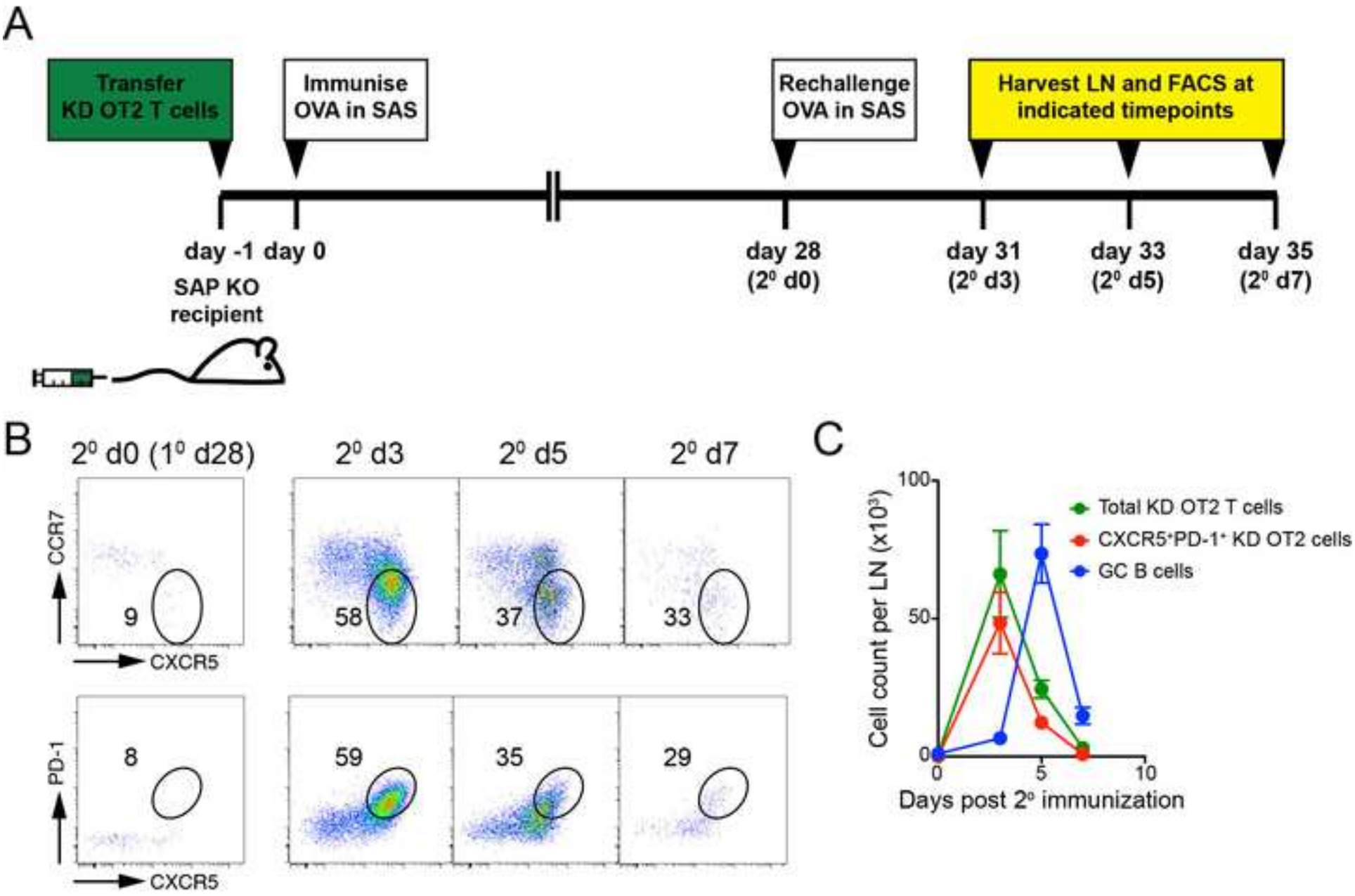

Supplemental Text & Figures

Click here to download high resolution image

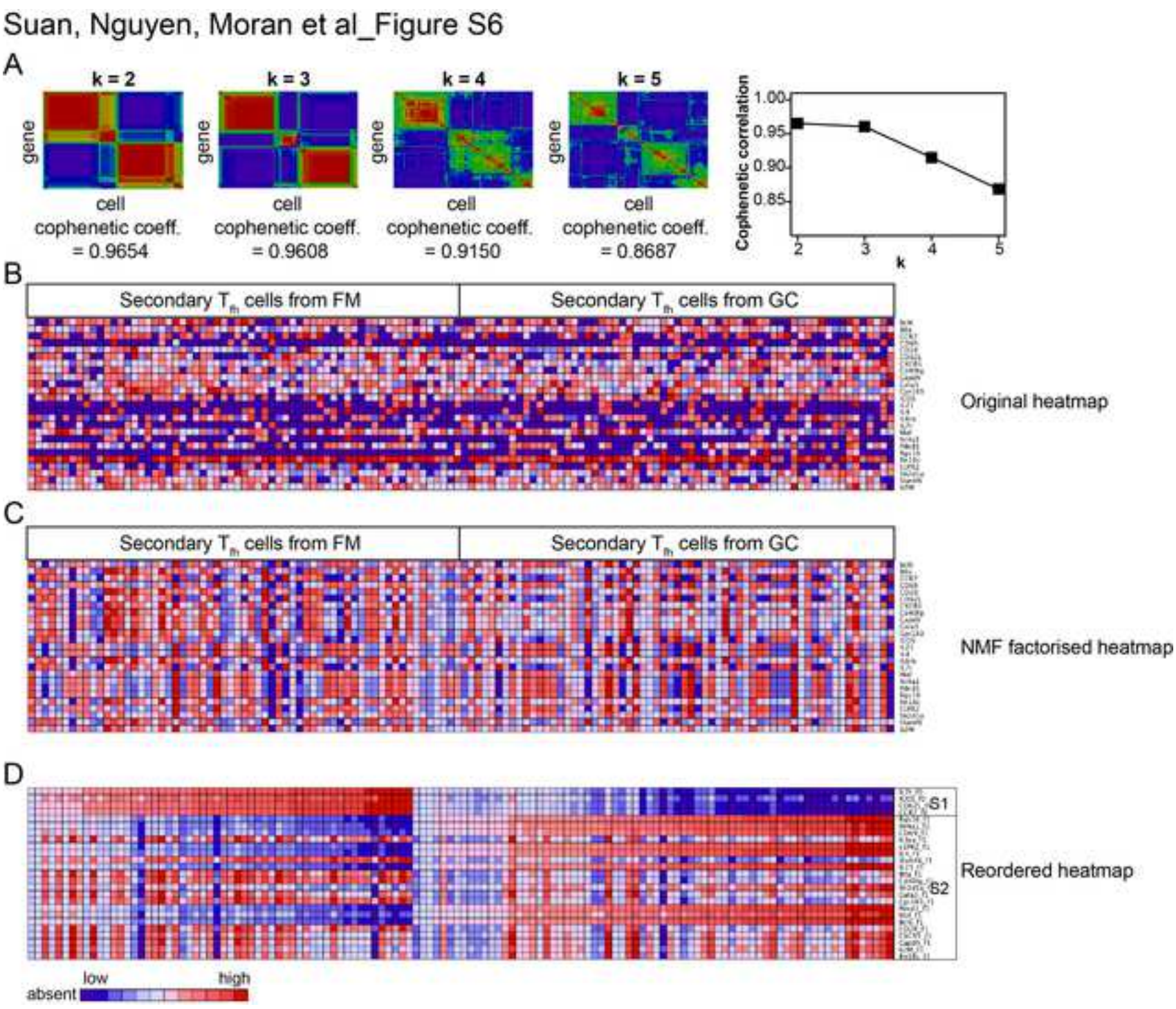

Supplemental Text & Figures

Click here to download high resolution image

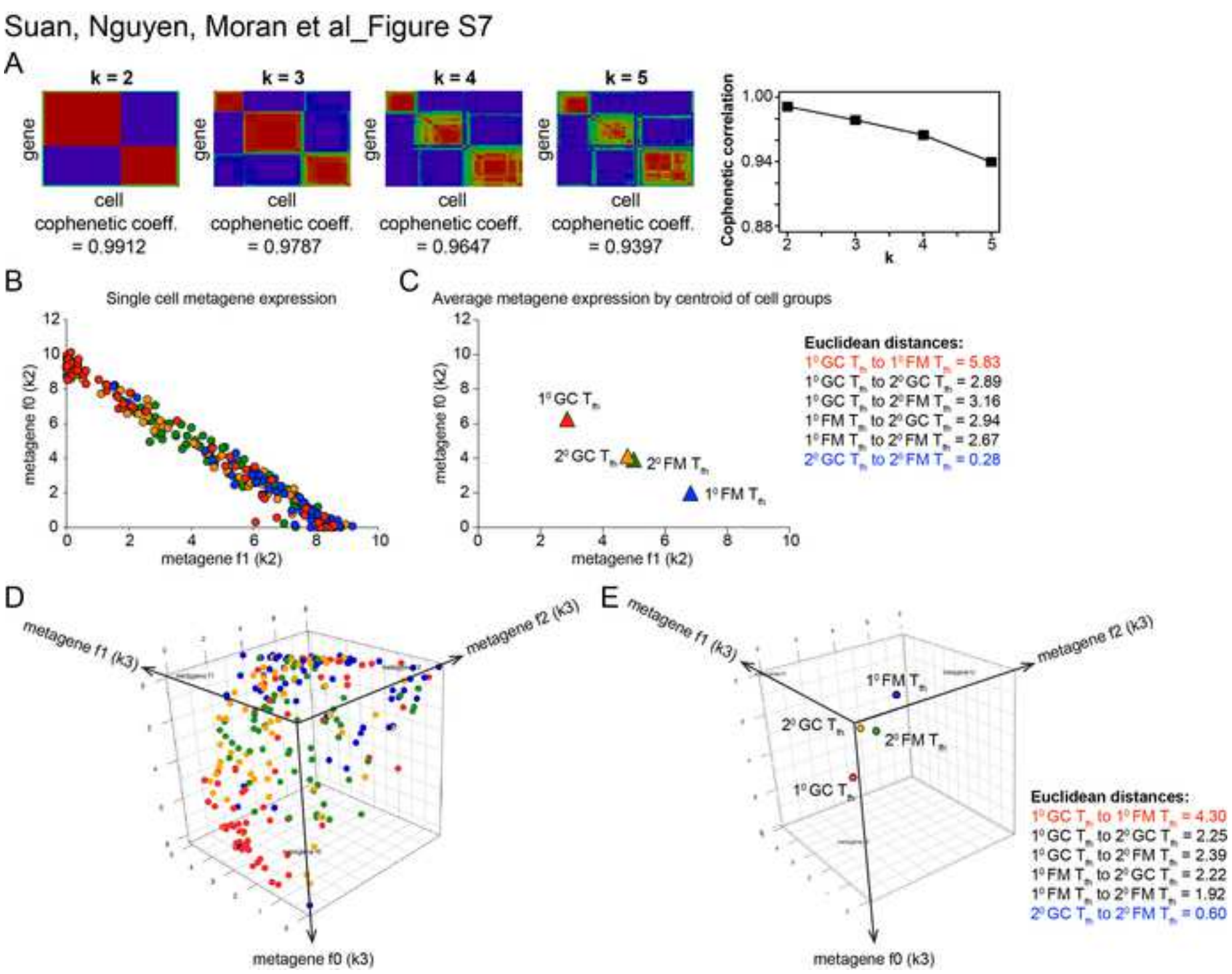

Supplemental Movies & Spreadsheets

Click here to download Supplemental Movies & Spreadsheets: Movie S1.mp4

Supplemental Movies & Spreadsheets

Click here to download Supplemental Movies & Spreadsheets: Movie S2.mp4

Supplemental Movies & Spreadsheets

Click here to download Supplemental Movies & Spreadsheets: Movie S3.mp4

Supplemental Movies & Spreadsheets

Click here to download Supplemental Movies & Spreadsheets: Movie S4.mp4

Supplemental Movies & Spreadsheets

Click here to download Supplemental Movies & Spreadsheets: Movie S5.mp4

Supplemental Movies & Spreadsheets

Click here to download Supplemental Movies & Spreadsheets: Movie S6.mp4

Supplemental Movies & Spreadsheets

Click here to download Supplemental Movies & Spreadsheets: Movie S7.mp4